

# Systematic Study of Confinement Induced Effects on Atomic Electronic Structure

Hugo Åström and Susi Lehtola\*

*University of Helsinki, Department of Chemistry, Faculty of Science, P.O. Box 55 (A.I. Virtanens plats 1), FI-00014 University of Helsinki, Finland*

E-mail: [susi.lehtola@alumni.helsinki.fi](mailto:susi.lehtola@alumni.helsinki.fi)

## Abstract

We point out that although a litany of studies have been published on atoms in hard-wall confinement, they have either not been systematic, having only looked at select atoms and/or select electron configurations, or they have not used robust numerical methods.

To remedy the situation, we perform in this work a methodical study of atoms in hard-wall confinement with the HELFEM program, which employs the finite element method (FEM) that trivially implements the hard-wall potential, guarantees variational results, and allows easily finding the numerically exact solution.

Our fully numerical calculations are based on non-relativistic density functional theory (DFT) and spherically averaged densities. We consider three levels of density functional approximations: the local density approximation employing the Perdew–Wang (PW92) functional, the generalized-gradient approximation (GGA) employing the Perdew–Burke–Ernzerhof (PBE) functional, and the meta-GGA approximation employing the r<sup>2</sup>SCAN functional. Importantly, the completely dissimilar density functional approximations are in excellent agreement, suggesting that the observed results are not artefacts of the employed level of theory.

We systematically examine low lying configurations of the H–Xe atoms and their monocations, and investigate how the configurations—

especially the ground state configuration—behave as a function of the position of the hard-wall boundary. We perform calculations with both spin-polarized as well as spin-restricted densities, and demonstrate that spin-polarization effects are significant in open shell configurations, even though some previous studies have only considered the spin-restricted model.

We demonstrate the importance of considering ground state changes for confined atoms by computing the ionization radii for the H–Xe atoms and observe significant differences to earlier studies. Confirming previous observations, we identify electron shifts on the outermost shells for a majority of the elements: valence *s* electrons are highly disfavored under strong confinement, and the high-lying 3*d* and 4*f* orbitals become occupied in atoms of periods 2–3 and 3–4, respectively.

We also comment on deficiencies of a commonly used density based estimate for the van der Waals (vdW) radius of atoms, and propose a better behaved variant in terms of the number of electrons outside the vdW radius that we expect will prove useful in future studies.

## 1 Introduction

The pioneering study of [Michels et al.](#)<sup>1</sup> was concerned on the question of how atomic polarizabilities—which have an important role in chemical bonding—evolve as a function of pressure. Published in 1937, the study exam-

ined the hydrogen atom enclosed in an impenetrable sphere of a variable radius to simulate pressure effects. Such frugal models offer a great tool for understanding basic physical effects precisely due to their simplicity: [Michels et al.](#)<sup>1</sup> found that hydrogen becomes less polarizable in increasing pressure, that is, when the radius of the sphere is decreased.

An interest in analogous studies of atoms in hard-wall confinement (i.e. atoms in a spherical box) continues to this day. A multitude of studies have been published on the very first atoms of the periodic table; see ref. [2](#) for a review dedicated to the H and He atoms confined by a finite or infinite spherical barrier with 200 references. Yet, few studies have considered many-electron atoms, or reported systematic calculations on the periodic table.

In hard-wall confinement, the wave function must vanish beyond the hard-wall boundary, and this can only be accomplished within a basis set with finite support. Many studies on confined atoms employing basis sets of an analytic form—such as Gaussian or Slater type orbital basis sets—have been published in the literature. However, these basis sets have finite tails in the forbidden region. Truncated Gaussian or Slater type orbital basis sets where this tail has been cut off do not have this issue, but they too suffer from basis set truncation errors (BSTEs), which are *a priori* unknown.

Our recent studies on atoms and molecules in strong magnetic fields found that changes in the electron configuration often resulted in significant increases in the BSTE of standard Gaussian-type orbital basis sets,<sup>3,4</sup> as these basis sets have not been optimized to describe electronic structure in this context. As we will discuss below, confinement is likewise expected to result in electron shifts to orbitals of higher angular momentum. Since this effect has again not been considered in the parametrization of standard Gaussian-type orbital basis sets, they cannot be expected to yield reliable estimates under confinement, since the orbitals of confined atoms can look extremely dissimilar to the orbitals of the unconfined atom. The qualitatively correct description of confinement induced effects then requires a careful study of

basis set convergence, ideally supplemented by comparisons to fully numerical reference values. We point out that few studies have attempted to reach the complete basis set limit, and we will report numerically exact complete basis set limit energies later on in this work.

Before laying out the scope of the present study, we will briefly review the literature we found that fulfills our key criteria at least in part: studies mentioned herein have examined atoms with more than 4 electrons, and employed a robust numerical method.

[Boeyens](#)<sup>5</sup> performed fully numerical Hartree–Fock calculations to determine the ionization radii of compressed atoms. However, [Boeyens](#)<sup>5</sup> did not employ a proper hard-wall potential. To approximate a hard-wall boundary at  $r = r_c$ , [Boeyens](#)<sup>5</sup> multiplied the wave function by the smooth step function  $\Theta(r) = \exp[-(r/r_c)^{20}]$  at every self-consistent field (SCF) iteration, before the normalization of the updated wave function was carried out. [Boeyens](#)<sup>5</sup> employed standard electron configurations for the elements, and thus did not consider changes in the occupations as a function of the confinement.

[Chattaraj and Sarkar](#)<sup>6</sup> employed a similar approach to that of [Boeyens](#)<sup>5</sup> in a density functional theory (DFT) study on chemical reactivity indices of the He–Ne and Br atoms, finding that the atoms become harder and less polarizable in increasing confinement, thus coming to the same conclusion as [Michels et al.](#)<sup>1</sup> in the case of hydrogen 66 years earlier. [Chattaraj and Sarkar](#)<sup>7</sup> also carried out a similar study for the reactivity indices for the He–Ne atoms and the  $C^+$ ,  $C^{2+}$ ,  $C^{3+}$ , and  $C^{4+}$  ions, with the same conclusion. Yet, it appears that [Chattaraj and Sarkar](#) did not consider the possibility of the electron configuration changing as a function of confinement in refs. [6](#) and [7](#).

[Sarkar et al.](#)<sup>8</sup> studied the effects of confinement on the chemical reactivity of the nitrogen atom. [Sarkar et al.](#)<sup>8</sup> compared the method of [Boeyens](#)<sup>5</sup> to the true hard-wall potential, and found the arising chemical reactivities to yield the same qualitative trends. Moreover, [Sarkar et al.](#)<sup>8</sup> found that different methods to calculate the reactivity yield dissimilar results, and that different electronic occupations also lead

to different chemical reactivities.

Connerade et al.<sup>9</sup> studied the filling of shells in the  $3d$  and  $4d$  elements as well as their cations in average-of-configurations Hartree–Fock calculations in a spherical cavity surrounded by a  $10E_h$  potential wall. They found that orbital filling becomes more regular for successive rows with increasing pressure, that is, when the finite barrier is placed closer and closer to the nucleus. In specific, the  $s$ – $d$  competition disappears for these elements, as the  $(n-1)d$  orbitals become energetically more favourable than the  $ns$  orbitals under confinement. Connerade and coworkers have also reported studies on some individual atoms under confinement. For instance, Connerade and Dolmatov<sup>10</sup> examined the Cr atom, while Connerade and Semaoune performed relativistic calculations on the La and Cs atoms in refs. 11 and 12, respectively.

A number of studies of atoms in hard-wall confinement have been carried out at the DFT level by Garza et al. Garza et al.<sup>13</sup> reported a finite differences method (FDM) implementation for solving the atomic DFT equations in the presence of a hard-wall boundary, and studied the Ne and Na (and He) atoms in exchange-only calculations. In a follow-up study, Garza et al.<sup>14</sup> examined the electrostatic potential of the unconfined and hard-wall confined Li, Na, K, and Rb atoms with DFT in order to study changes in the atoms’ shell structure, and found that shell structure is gradually lost in increasing confinement. Similarly, Sen et al.<sup>15</sup> determined atomic ionization radii for the He–Ca atoms with hard-wall confined DFT calculations. As none of the studies by Garza et al.<sup>13</sup>, Garza et al.<sup>14</sup>, or Sen et al.<sup>15</sup> discuss occupations, we can only assume that the ground state electron configuration of the unconfined atom was used in their calculations. In contrast, the study on the chemical reactivity indices of the compressed Li, Na, and K; Be, Mg, and Ca; N, P, and As; and Ne, Ar, and Kr atoms by Garza et al.<sup>16</sup>, which was likewise carried out with hard-wall confined DFT, explicitly mentions finding the lowest electron configuration for each confinement radius.

Continuing with the Garza group, Guerra et al.<sup>17</sup> modeled pressure effects on the elec-

tronic properties of Ca, Sr, and Ba with hard-wall confined DFT, and found that their ground state changes from the  $ns^2$  configuration to the  $ns^1(n-1)d^1$  and  $ns^0(n-1)d^2$  configurations in increasing pressure. Confinement effects on the spin potential of first-row transition metal cations were investigated at the hard-wall confined DFT level of theory by Lozano-Espinosa et al.<sup>18</sup>.

Pašteka et al.<sup>19</sup> studied the C and K (and He) atoms in hard-wall confinement with the finite element method (FEM) at the complete active space self-consistent field<sup>20,21</sup> (CASSCF) level of theory, which represents the most sophisticated level of theory in the studies we found. Also Pašteka et al.<sup>19</sup> found changes in atomic ground state configurations under confinement: the ground state configuration of carbon changes from  $1s^22s^22p^2$  in the free atom to  $1s^22p^4$  in strong confinement.

As this literature overview demonstrates, although several fully numerical studies have been published on atoms in confinement, they have mostly focused on small groups of similar atoms. The study of Boeyens<sup>5</sup> was the most complete, considering non-relativistic calculations on the first 105 atoms of the periodic table, but the study relied on an *ad hoc* implementation of confinement, and—like in many other studies mentioned above—changes in the ground state as a function of confinement were not considered. Studies that considered changes in the ground state are likewise limited: Connerade et al.<sup>9</sup> only considered  $3d$  and  $4d$  elements, Garza et al.<sup>16</sup> studied only atoms of groups 1, 2, 15, and 18, and Guerra et al.<sup>17</sup> only studied heavy atoms of group 2.

The only study that appears to have systematically investigated effects of confinement on the electronic structure of atoms so far is the study of Rahm et al.<sup>22</sup>, which employed the extreme pressure polarizable continuum model<sup>23</sup> (XP-PCM) to study the first 93 atoms under pressure, employing the ANO-RCC Gaussian basis set<sup>24</sup> with scalar relativistic corrections and the 25% hybrid<sup>25,26</sup> of the Perdew–Burke–Ernzerhof (PBE) functional,<sup>27,28</sup> which is commonly known as PBE0. Rahm et al.<sup>22</sup> identified electron shifts,  $s \rightarrow p$ ,  $s \rightarrow d$ ,  $s \rightarrow f$ ,

and  $d \rightarrow f$ , as essential chemical and physical consequences of compression. In follow-up work, [Rahm et al.](#)<sup>29</sup> studied non-bonded radii of compressed atoms with analogous calculations. [Rahm et al.](#)<sup>22</sup> and [Rahm et al.](#)<sup>29</sup> did not report carrying out a basis set convergence study of their findings. Yet, as already discussed above, Gaussian basis sets cannot be expected to deliver reliable results in strong confinement.<sup>19</sup>

As is clear from the above discussions, there is a hole in the literature regarding systematic fully numerical studies covering (a significant fraction of) the periodic table. Changes in the electronic structure of atoms are an expected effect of confinement, and they thus need to be taken into account by considering changes in the electronic occupations as a function of confinement. Fully numerical techniques are critically important as changes in the electronic occupations cannot be expected to be adequately reproduced by standard Gaussian-type orbital basis sets, for example.

In this work, we will address this major shortcoming of the existing literature with a systematic study on atoms in hard-wall confinement within a fully numerical approach, while also thoroughly considering the effect of the confinement on the ground state electron configuration.

Our results confirm previous partial findings of the fully numerical studies of [Connerade et al.](#)<sup>9</sup>, [Guerra et al.](#)<sup>17</sup>, and [Pařteka et al.](#)<sup>19</sup> as well as the thorough Gaussian basis study of [Rahm et al.](#)<sup>22</sup>: confinement induced electron shifts can be observed for a majority of the elements. It is important to note here that all of these studies have been carried out with different methodologies. Furthermore, as we shall see, the dissimilar functionals we employ in this work are all in good agreement. This suggests that the findings of this work indeed correspond to physical effects of confinement despite the arguably simplistic level of theory employed herein.

The layout of this work is the following. The theory behind the present work is briefly discussed in section 2. The form of the Hamiltonian including the hard-wall potential and the employed DFT approach is discussed in sec-

tion 2.1. The employed theories for calculating ionization energies and ionization radii are discussed in sections 2.2 and 2.3, respectively. As our study includes data on a variety of electron configurations, we discuss ways to estimate the corresponding atomic radii in section 2.4, where we also introduce a new way to estimate atoms' van der Waals (vdW) radii. Next, the computational details including the employed numerical approach are presented in section 3. The results are presented in section 4. We first demonstrate that our method works by computing ionization energies and ionization radii in sections 4.1 and 4.2, respectively. Then, we analyze the numerical and physical behavior of the employed vdW radius estimates in section 4.3 and find our vdW estimate to address many issues in a commonly used estimate. The highlights from our analysis of the behavior of the low lying configurations of the H–Xe atoms in hard-wall confinement are presented in section 4.4. The article concludes in a summary and discussion in section 5. Atomic units are employed throughout the work. The full set of raw data as well as a detailed analysis of the results is included in the Supporting Information (SI).

## 2 Theory

### 2.1 DFT approach

The Hamiltonian for the confined atoms reads

$$\hat{H} = \hat{H}_0 + V_c(r), \quad (1)$$

where

$$\hat{H}_0 = -\frac{1}{2} \sum_i \nabla_i^2 - \sum_i \frac{Z}{r_i} + \sum_{i < j} \frac{1}{|\mathbf{r}_i - \mathbf{r}_j|} \quad (2)$$

is the standard electronic Hamiltonian for an atom with atomic number  $Z$ , and  $V_c(r)$  is the potential for a hard-wall boundary at  $r_c$

$$V_c(r) = \begin{cases} 0, & r < r_c \\ \infty, & r \geq r_c. \end{cases} \quad (3)$$

As already mentioned in section 1, we carry out calculations on many-electron atoms within

the context of DFT.<sup>30,31</sup> We expand the one-particle states also known as atomic orbitals (AOs) in a numerical basis set as

$$\chi_{nlm}^\sigma(\mathbf{r}) = R_{nl}^\sigma(r)Y_{lm}(\hat{\mathbf{r}}), \quad (4)$$

where  $Y_{lm}(\hat{\mathbf{r}})$  are spherical harmonics; we will discuss the form of the radial expansion  $R_{nl}^\sigma(r)$  below in section 3.

Following standard practice in numerical DFT calculations on atoms, we assume that the electron density is spherically symmetric,  $n_\sigma(\mathbf{r}) = n_\sigma(r)$  for each spin  $\sigma$ . This simplification leads to an efficient algorithm, since the problem of solving the Kohn–Sham equations,<sup>31</sup> i.e., the optimization of the  $s$ ,  $p$ ,  $d$ , and  $f$  orbitals becomes a set of coupled one-dimensional problems.<sup>32,33</sup>

Furthermore, we will assume integer occupations on the  $s$ ,  $p$ ,  $d$  and  $f$  shells in the aim to extract chemical understanding from the calculations. These integer occupations are then averaged over all magnetic sublevels to produce spherically symmetric total densities; this leads to fractional occupations on the individual spatial orbitals. The electron density is thus given simply as

$$n_\sigma(r) = \frac{1}{4\pi} \sum_{nl} f_{nl}^\sigma [R_{nl}^\sigma(r)]^2, \quad (5)$$

where  $f_{nl}^\sigma$  is the number of spin- $\sigma$  electrons on the  $nl$  shell. The occupations  $f_{nl}^\sigma$  are determined from the number of electrons with angular momentum  $l$  using Hund’s rules: the orbitals are filled starting from  $n = l + 1$  by occupying the  $2l + 1$  spin-up orbitals for the given  $n$  before occupying the corresponding  $2l + 1$  spin-down orbitals. We refer to refs. 32 and 33 for further discussion.

The above choice of theory has both a physical and a practical rationale. The fractional occupation formalism automatically guarantees spherical degeneracy,<sup>32,33</sup> since all magnetic sublevels are assumed to behave identically. In contrast, DFT calculations with integer occupations of the magnetic sublevels often break spatial symmetry and fail to reproduce the degeneracy of atomic multiplets.<sup>32</sup> Although sev-

eral specialized approaches to reproduce atomic multiplets within a DFT style description have been proposed,<sup>34–38</sup> they appear to be quite involved and have not gained wide adoption. We also wish to direct the reader to the discussion of Baerends et al.<sup>39</sup> on atomic reference energies for DFT calculations.

## 2.2 Ionization energies

Within the above level of theory, atoms’ ionization energies can be calculated in two ways. First, in the  $\Delta$ SCF method the ionization energy is determined for each value of  $r_c$  as the difference between the total energy of the cation and of the neutral atom

$$E_+(r_c) = E_{\text{cation}}(r_c) - E_{\text{neutral atom}}(r_c). \quad (6)$$

As is discussed below in section 3, the calculations on unconfined atoms employ the value  $r_c = 40a_0$  which is large enough to afford fully converged energies for the ground states of atoms and their cations.

Second, Boeyens<sup>5</sup> used Koopmans’ theorem<sup>40</sup> to determine the ionization radii. While there is no Koopmans’ theorem for DFT as in Hartree–Fock, Janak’s theorem<sup>41</sup> provides a justification for an analysis based on orbital energies. The ionization energy is determined via Janak’s theorem as

$$E_+(r_c) = -\epsilon^{\text{H}^{\text{OAO}}}(r_c), \quad (7)$$

where  $\epsilon^{\text{H}^{\text{OAO}}}(r_c)$  is the eigenvalue of the highest occupied atomic orbital (H<sup>O</sup>AO) of the neutral atom with the hard-wall boundary at  $r = r_c$ .

## 2.3 Ionization radii

Now that we have defined ways to calculate ionization energies, we can calculate ionization radii for atoms, i.e., the location of the hard-wall boundary where the atom favors casting away its outermost electron. The ionization radius  $r_+$  for atom X is by solving the nonlinear equation

$$E_+(r_c) = 0. \quad (8)$$

If the ionization energy is computed with eq. (6), eq. (8) is straightforward to solve to

high precision by bisection, once a crossing between the atomic and cationic curves has been identified. Now, the issue becomes that the energy of the atom in its neutral and cationic charge state depends on the employed electron configuration. This issue can be approached in two ways. The first is to follow the work of Boeyens<sup>5</sup> and many others (see section 1) and fix the electron configuration to that of the ground state of the unconfined neutral atom and its monocation, respectively. The second is to realize that confinement can affect the ground state configurations of the atom and its cation, and to compute the energies  $E_{\text{neutral atom}}(r_c)$  and  $E_{\text{cation}}(r_c)$  for the lowest configurations of the neutral atom and cation, respectively, at each value of  $r_c$ .

Alternatively, we can use the estimate from Janak’s theorem of eq. (7) to solve eq. (8). Again, one can choose to use the electron configuration of the ground state of the unconfined neutral atom, or to employ a relaxed configuration at every value of  $r_c$ . However, exact solution to eq. (8) is sometimes problematic in the latter case. A case in point is the V atom: the value of  $r_+$  corresponds to the location of a ground state crossing between a state with  $\epsilon^{\text{HOMO}}(r) < 0$  and a state with  $\epsilon^{\text{HOMO}}(r) > 0$ , which means that eq. (8) is not truly satisfied no matter how tightly  $r_+$  is converged.

The origin of the above problem is the present use of electron configurations with integer occupations. However, it has long been known that the use of non-integral occupation numbers for the 4s and 3d shells can result in a lower total energy for transition metal atoms in average-of-configurations Hartree–Fock calculations.<sup>42</sup> This phenomenon is also topical for the present DFT calculations,<sup>32,43</sup> and has also been found in DFT calculations that do not employ any exchange-correlation functional.<sup>44</sup> Calculations employing variationally optimized fractional occupation numbers would allow finding an exact solution to eq. (8), likely producing a slightly different radius. However, we do not consider such fractional occupations in this work, since integer occupation numbers are more commonly used and allow a clearer physical interpretation of the results.

## 2.4 Atomic radii

The location of the density maximum of the outermost orbital is a long-established estimator for the size of covalently bound atoms<sup>45</sup>

$$r_{\text{max}} = \max_i \left( \operatorname{argmax} [r^2 n_i(r)] \right), \quad (9)$$

where  $n_i(r)$  is the  $i$ th orbital density.

Since the electron density of an atom decays in the far valence region, a density threshold can be used to estimate the atom’s van der Waals (vdW) radius<sup>46</sup>

$$n(r_\rho) = \epsilon, \quad (10)$$

where the electron density was defined above in eq. (5), and the solution of eq. (10) with a given threshold  $\epsilon$  defines the vdW radius estimate  $r_\rho$ .

Due to several issues related to eq. (10) discovered and discussed in detail later in this work (for instance, eq. (10) does not have a solution in some cases, leaving the vdW radius undefined), we propose another metric for the vdW radius in this work. The vdW radius can be determined by containing all the electrons of the atom except  $\epsilon$  within the volume enclosed by that radius,

$$4\pi \int_{r_\epsilon}^{\infty} n(r) r^2 dr = \epsilon, \quad (11)$$

where the electron density is again defined by eq. (5). This metric is well defined for any configuration of any element, and also exhibits superior numerical stability over eq. (10); see section 4.3 for discussion. Equation (11) is also straightforward to extend to non-spherically symmetric electron densities as

$$\int_{r_\epsilon}^{\infty} r^2 dr \int n(\mathbf{r}) d\Omega = \epsilon, \quad (12)$$

which will be relevant for applications with the CASSCF method, for instance.

## 3 Computational Details

FEM offers a straightforward way to the numerical solution of the radial functions  $R_{nl}^\sigma$ ;<sup>47</sup>

a review of the employed FEM approach can be found in refs. 48 and 49. In short, the radial domain is first divided into  $N_{\text{elem}}$  segments  $r \in [r_i^{\text{start}}, r_i^{\text{end}}]$  called elements. An exponential radial grid  $\{r_i\}_{i=0}^{N_{\text{elem}}}$  is employed, so that the size of the elements increases with the distance from the nucleus.<sup>48,49</sup> A piecewise polynomial basis of shape functions  $B_n(r)$  is then built up in each element.<sup>48,49</sup> Finally, the numerical radial basis functions to be used in eq. (4) are built from FEM shape functions  $B_n(r)$  as

$$R_n(r) = r^{-1}B_n(r), \quad (13)$$

and the same radial basis set is used for all angular momenta  $l$ . This approach is robust and allows maximal flexibility: as the basis functions within one element have zero overlap to basis functions in other elements, the spatial representation can be adaptively refined, if necessary.

The endpoint of the last element is called the practical infinity,  $r_\infty$ , and all basis functions are built to vanish at  $r_\infty$ .<sup>48,49</sup> The physical interpretation of  $r_\infty$  is that there is a hard-wall potential at this point; eq. (3) is therefore already built-in in the FEM approach, and this feature has been previously used in many studies, such as refs. 19 and 49. Thus,  $r_\infty$  represents a physical parameter that expresses the location of the hard-wall boundary. In contrast, in studies of unconfined atoms (which represent the typical applications of FEM in the literature),  $r_\infty$  is a discretization parameter that needs to be converged such that the obtained solution does not change if an even larger value is employed for  $r_\infty$ .

As our main focus is on atoms in confinement, the calculations unconfined atoms employed the default value  $r_\infty = 40a_0$ , which is sufficient to reproducing the complete basis set limit energy of the ground states of neutral atoms and their cations. We note here that as larger values of  $r_\infty$  may be necessary to capture the behavior of loosely bound states, energies of the excited states in unconfined atoms may not be converged to the complete basis set limit with respect to this parameter. In contrast, the energies for the excited states in the confined atoms

are converged to the complete basis set limit, as is explained below.

All calculations in this work were carried out with the free and open-source<sup>50</sup> HELFEM program; the present implementation is publicly available on GitHub.<sup>51</sup> The calculations employed shape functions defined by 15-node Lagrange interpolating polynomials (LIPs) specified by Gauss–Lobatto quadrature nodes; this corresponds to the use of a 14<sup>th</sup> order polynomial basis set. All calculations were converged to the complete basis set (CBS) limit with respect to the number of radial elements: radial elements were added until a  $1\mu E_h$  precision in the total energy was achieved. We can thus be assured that we have found the numerically exact wave function.

We employ the optimal FEM implementation of the fractional occupation formalism recently described in refs. 32 and 33. We perform calculations within the local density approximation<sup>52,53</sup> employing the Perdew–Wang (PW92) correlation functional,<sup>54</sup> within the generalized-gradient approximation (GGA) employing the Perdew–Burke–Ernzerhof (PBE) exchange-correlation functional,<sup>27,28</sup> and within the meta-GGA approximation employing the r<sup>2</sup>SCAN exchange-correlation functional,<sup>55,56</sup> all as implemented in LIBXC<sup>57</sup> using the `lda_x-lda_c_pw`, `gga_x_pbe-gga_c_pbe`, and `mgga_x_r2scan-mgga_c_r2scan` keywords, respectively.

We initiated the work by identifying the three lowest lying configurations of all elements with atomic number  $1 \leq Z \leq 54$  in the hard-wall potential for each  $r_c \in \{1.0, 1.2, 1.4, \dots, 10.0\}a_0$  with both spin-restricted and spin-polarized densities, respectively, with a fixed angular momentum cutoff  $l_{\text{max}} = 3$ . The configurations were determined with the automated algorithm introduced in ref. 32. The configurations considered for the spin-(un)restricted analysis were then chosen as the union of the low-lying configurations obtained from the spin-(un)restricted search over all of the above values of  $r_c$ .

We checked whether  $g$  orbitals would become occupied for heavy atoms by repeating the configuration search for the Rb and Xe atoms with  $l_{\text{max}} = 4$ . However, no configurations with oc-

cupied  $g$  orbitals were obtained in this search.

The configuration search above was performed with the PBE functional, only. However, as we shall see in section 4, the results are qualitatively independent of the employed density functional approximation. For this reason, we are confident that our search yielded all relevant configurations for the PW92 and r<sup>2</sup>SCAN functionals, as well.

Thus being convinced to have found the low-lying configurations for the H–Xe atoms, we performed calculations on all these configurations with  $r_c \in \{1.0, 1.1, \dots, 10.0\}a_0$ . The wide range of studied values of  $r_c$  allows us to observe many interesting evolutions. The states with  $r_c = 10.0a_0$  are similar to those of the unconfined atom, while  $r_c = 1.0a_0$  represents extreme confinement where even core orbitals experience confinement effects and the valence electrons are bound only by the confinement potential.

## 4 Results

### 4.1 Ionization energies of unconfined atoms

As a first step to validate our methods we compute ionization energies for the unconfined H–Xe atoms in the spin-restricted and spin-polarized formalisms according to the two methods discussed in section 2.2.

As the three dissimilar functionals yield ionization energies that are all in good agreement with the experimental data, we only discuss the PBE data here. The comparison of our PBE values to the experimental values of [Kramida et al.](#)<sup>58</sup> is depicted in fig. 1; analogous plots for the PW92 and r<sup>2</sup>SCAN functionals are included in the SI.

The values obtained from Janak’s theorem are consistently and significantly lower than the experimental values and we will therefore not discuss them further.

The  $\Delta$ SCF formalism produces ionization energies in good agreement with experiment. As expected, the results of the spin-polarized calculations are in better agreement with exper-

iment than those from the spin-restricted calculations. Notable differences can be observed already for the H and He atoms. Spin-polarized calculations also faithfully reproduce the dip in the ionization energy beyond half filling of the  $p$  shell, while spin-restricted calculations predict that the ionization energy increases monotonically with the filling of the  $p$  shell.

### 4.2 Ionization radii

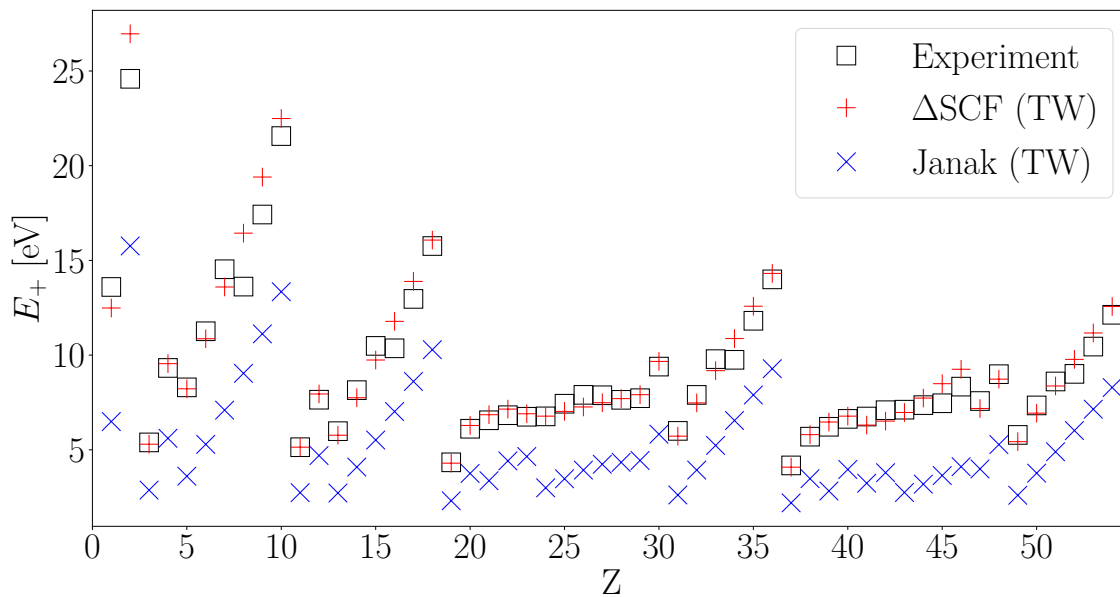
#### 4.2.1 $\Delta$ SCF

As discussed in section 2.3,  $\Delta$ SCF ionization radii can be computed in two ways. In the first method we fix the configurations to those of the ground state of the neutral atoms and their cations, respectively. In the second method we relax the configurations of the atoms and cations to the lowest configurations at each radius. The resulting ionization radii for the H–Xe atoms obtained with the PBE functional are shown in table 1 and its insert, respectively, when the second method predicts a different ionization radius than the fixed configuration approach.

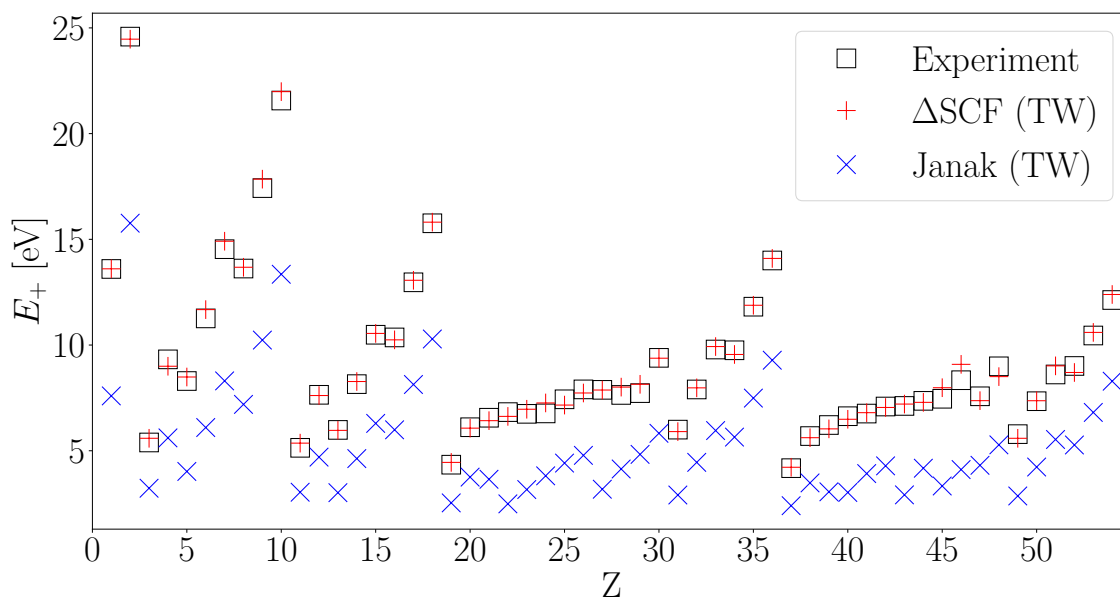
The ionization radius for the hydrogen atom is an interesting place to start the analysis. The corresponding exact model is analytically solvable: [Sommerfeld and Welker](#)<sup>59</sup> obtained the ionization radius  $1.8352a_0$  in their pioneering study. The exact ground state of hydrogen is fully spin polarized and our spin-polarized PW92, PBE and r<sup>2</sup>SCAN values of  $1.90a_0$ ,  $1.86a_0$ , and  $1.84a_0$  deviate from the exact value by only 4.5%, 1.4% and 0.3%, respectively. The spin-restricted values of  $1.99a_0$ ,  $1.95a_0$ , and  $1.96a_0$  exhibit much larger deviations of 8.4%, 6.3%, and 6.8 %, respectively, but are still remarkably accurate considering that our spin-restricted calculations are for an atom with 1/2 spin-up and 1/2 spin-down electrons.

Moving on to heavier elements, the comparison of the results from the fixed electron configuration and relaxed configuration methods proves interesting. Although inclusion of the relaxation effects does not appear to be important for most of the studied elements, large differences are observed in the pre- $d$  and  $d$  blocks





(a) Ionization energies of the H–Xe atoms obtained with the PBE functional and spin-restricted densities.



(b) Ionization energies of the H–Xe atoms obtained with the PBE functional and spin-polarized densities.

Figure 1: Comparison of the ionization energies of unconfined atoms computed with spin-restricted (fig. 1a) and spin-polarized (fig. 1b) densities in this work (TW) with  $\Delta$ SCF or Janak’s theorem against experimental values of [Kramida et al.](#)<sup>58</sup>.

H	1.95																				He	1.34
Li	1.85																				Ne	1.40
		Be	3.14																		F	1.96
			3.21																		O	2.15
																					N	2.28
Na	4.06																				P	3.28
		Mg																			Si	3.64
			3.70																		S	2.99
			3.76																		Cl	2.75
K	5.26																				Ar	2.56
		Ca	4.82																		Sc	2.57
			4.77																		Ti	3.28
																					V	3.18
Rb	5.56																				Cr	3.34
		Sr	5.12																		Mn	3.71
			5.07																		Fe	3.62
																					Co	3.71
																					Ni	3.44
																					Cu	3.34
																					Zn	3.34
																					Ga	3.83
																					Ge	3.62
																					In	4.09
																					Cd	4.41
																					Pb	3.66
																					Bi	3.84
																					Po	3.10
																					At	3.29
																					Hg	3.51
																					Tl	3.79
																					Pb	4.17
																					Bi	4.17
																					Po	3.83
																					At	3.88
																					Rn	3.88
																					Fr	3.88
																					Ra	3.88
																					Ac	3.27
																					Th	3.28

Table 1: Ionization radii  $R$  in  $a_0$  for the H–Xe atoms from spin-restricted (in red) and spin-polarized (in blue) non-relativistic  $\Delta$ SCF calculations with fractional occupancies and the PBE functional with configurations fixed to the ground states of the unconfined neutral atom and its cation. Values obtained while considering the  $R$  dependence of the ground state of the neutral atom and its cation are highlighted in the insert for the elements where the value differs from the static configurations.

of the periodic table (Ca–Ni and Sr–Ru).

Since relaxing the configuration can result in a considerable decrease of the energy of the neutral atom, the second method is naively expected to yield ionization radii that are considerably smaller than the radii obtained with the first method of examining fixed electron configurations for the neutral atom and its cation. As expected, allowing the configuration to relax results in significant decreases in the ionization radii for most transition metals: for instance, the ionization radius of Mo decreases by 13% in the spin-restricted calculations when changes to the ground state of Mo and Mo<sup>+</sup> are considered (the spin-polarized change is just  $-1.4\%$ ). Similarly, the spin-polarized calculation on Ru leads to an ionization radius that is 13% smaller when the electron configuration is allowed to relax (no change in the spin-restricted calculation).

However, significant changes in energy upon relaxing the configuration may also occur for the cation, in which case the ionization radius can increase. Interestingly, such increases when the ground states are relaxed *are* observed for the Ca, Sc, and Sr atoms in both the spin-restricted and spin-polarized cases, as well as the Y atom in the spin-restricted case. The corresponding cations exhibit a ground state crossing that moves the cross-over point of eq. (8) down in energy, and thereby the ionization radius to the right; see fig. 2 for an illustration of these four exceptional cases.

Because the various configurations' energies span several orders of magnitude under the studied range of confinement radii, we compare the energy of the confined atom with electron configuration  $i$  to that of the ground state configuration of the unconfined atom

$$\Delta E_i(r_c) = E_i(r_c) - E_0^{\text{unconfined}}, \quad (14)$$

where  $i$  is the state in question in all plots in this study.

The differences observed in ionization radii with and without relaxing the electron configuration underline the importance of considering all possible low lying configurations as a function of confinement. Many transition metal

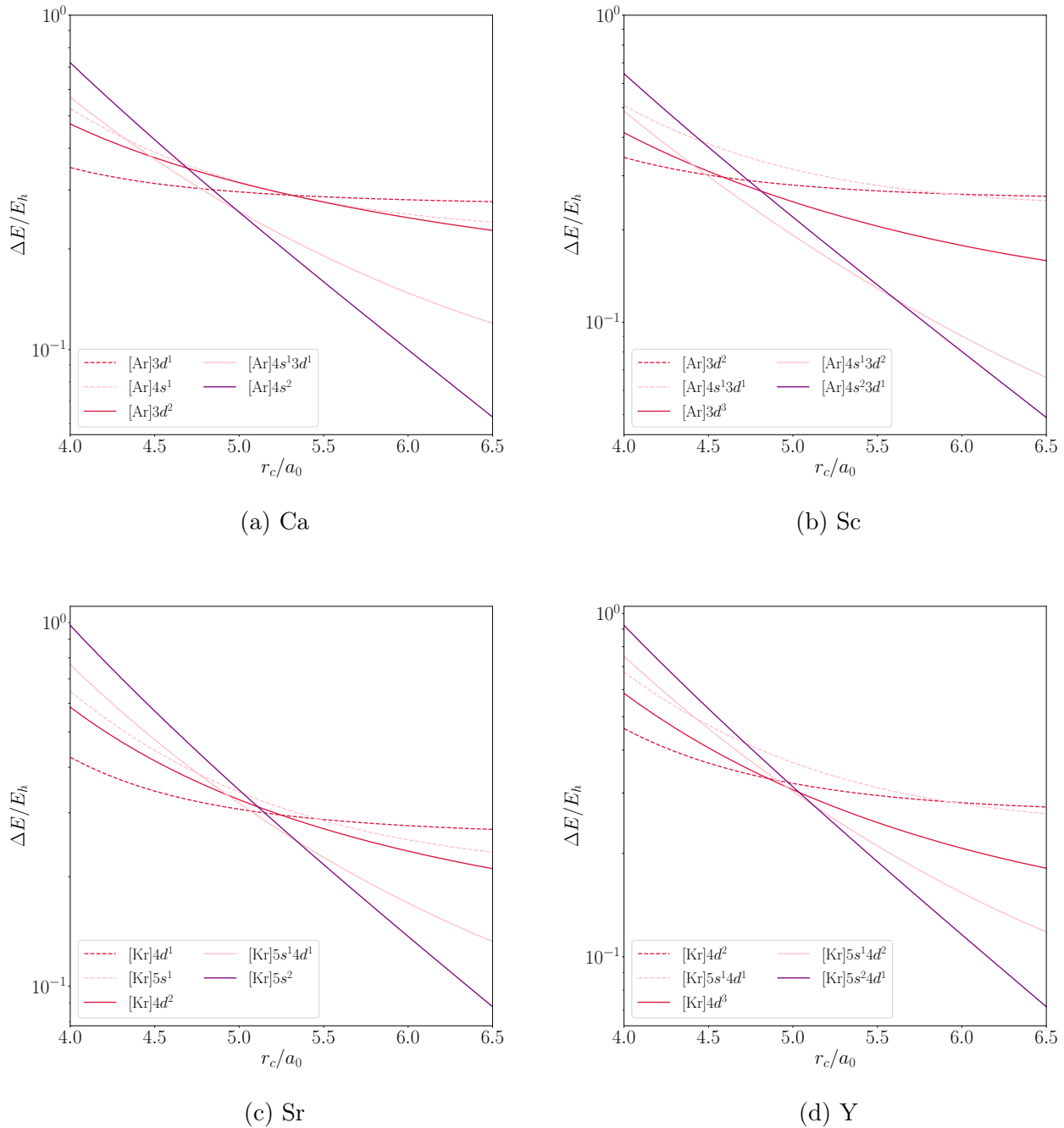


Figure 2: Ground state crossings for the spin-polarized Ca, Sc and Sr atoms, and the spin-restricted Y atom in the hard-wall potential with the PBE functional. Configurations for the neutral atoms shown as solid lines, and those corresponding to the monocation as dashed lines.

atoms and their monocations exhibit ground state crossings already in weak confinement, due to the low-lying  $s$ - $d$  excitations in these systems (see section 4.4).

The spin-polarized and spin-restricted ionization radii differ for all atoms, which is not surprising given that either the neutral atom or its cation is going to be open-shell. Interestingly, the differences between these two approaches are the smallest for the noble gas atoms, while alkali metals show much larger differences between spin-polarized and spin-unpolarized calculations. As the spin-polarized calculations gave ionization energies in best agreement with experiment in section 4.1, the spin-polarized ionization radii should be the most accurate.

A comparison of the ionization radii obtained with the PW92, PBE and r<sup>2</sup>SCAN functionals with spin-polarized densities and relaxed configurations is shown in fig. 3. Except for the alkali metals, as well as the Cr, Y, and Nb atoms, the dissimilar density functional approximations are in excellent agreement. We further validate this agreement by qualitatively studying the functional dependence of the behavior of all low lying configurations of the Ca atom in figs. 4 to 6, while the graphical representation of the results of the other atoms is included in the SI. We chose to feature Ca here due to its interesting chemistry which will be discussed below in section 4.4. The only major difference between the functionals is that r<sup>2</sup>SCAN predicts the  $4s^1 3d^1$  configuration to be lower in energy than the  $4s^1 4p^1$  configuration in the unconfined atom, while PW92 and PBE predict the opposite.

Despite such minor differences in the ordering of some states, or relative energy differences between states, the qualitative behaviors obtained with the three different density functional approximations agree well with each other; the changes in the electron configurations are practically independent of the functional. This suggests that the phenomena found with the methodology employed in this work are not artefacts of the used level of theory, but true physical phenomena within the studied model of confinement.

### 4.2.2 Janak’s theorem

We report ionization radii obtained from calculations using Janak’s theorem as tables in the SI, as we already found above in section 4.1 that these calculations failed to reproduce ionization energies in a reliable manner.

Sen et al.<sup>15</sup> computed atomic ionization radii with Janak’s theorem for the He–Ne atoms with exchange-only calculations based on Becke’s 1988 generalized-gradient functional.<sup>60</sup> In contrast to our work, Sen et al.<sup>15</sup> employed the transition state approximation (TSA) of Slater et al.<sup>42</sup> in their calculations; the orbital energies were thus determined in calculations where half an electron was removed from the highest-lying orbital. Sen et al.<sup>15</sup> compared this method to  $\Delta$ SCF calculations and found that the two methods yield ionization radii in close agreement to each other. Despite the differences between our approaches, we will see below that our results are in good agreement with those of Sen et al.<sup>15</sup>.

### 4.2.3 Comparison to literature radii

Numerically reliable ionization radii have been previously published by Boeyens<sup>5</sup>, Sen et al.<sup>15</sup>, and Garza et al.<sup>16</sup>. We compare our ionization radii from calculations based on the  $\Delta$ SCF method (section 4.2.1) and Janak’s theorem (section 4.2.2) with relaxed configurations and the PBE functional against the earlier calculations in fig. 7. Analogous plots for the PW92 and r<sup>2</sup>SCAN functionals can be found in the SI. We note that the dip in energy for the group 16 elements, which was found in the ionization energies in section 4.1, is also visible in the ionization radii in fig. 7.

We first note that the analysis of Boeyens<sup>5</sup> was based on non-relativistic Hartree–Fock calculations for  $1 \leq Z \leq 102$ , and  $r_+$  was identified via Koopmans’ theorem<sup>40</sup> by finding the zero of the orbital energy of the outermost valence electron shell. However, as discussed in section 1, Boeyens<sup>5</sup> did not employ a proper hard-wall potential, and did not consider the changing nature of the ground state configuration as a function of confinement. The values of Boeyens<sup>5</sup> are systematically and considerably larger than

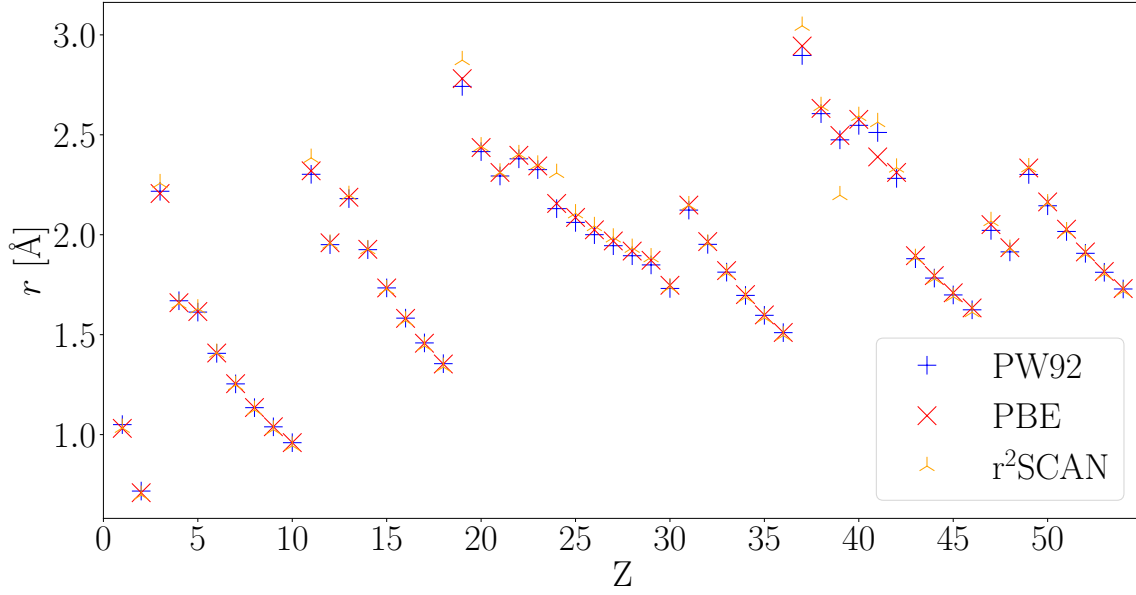


Figure 3: Ionization radii for the H–Xe atoms with the PW92, PBE and  $r^2$ SCAN functionals obtained from spin-polarized densities via  $\Delta$ SCF with relaxed configurations.

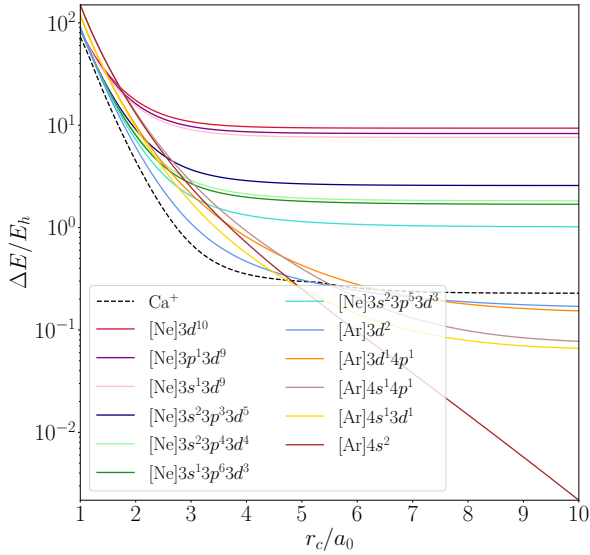


Figure 4: Energies of low lying configurations of hard-wall confined spin-polarized Ca computed with PW92 shown as the energy difference from unconfined Ca as a function of the confinement radius. Note semilogarithmic scale.

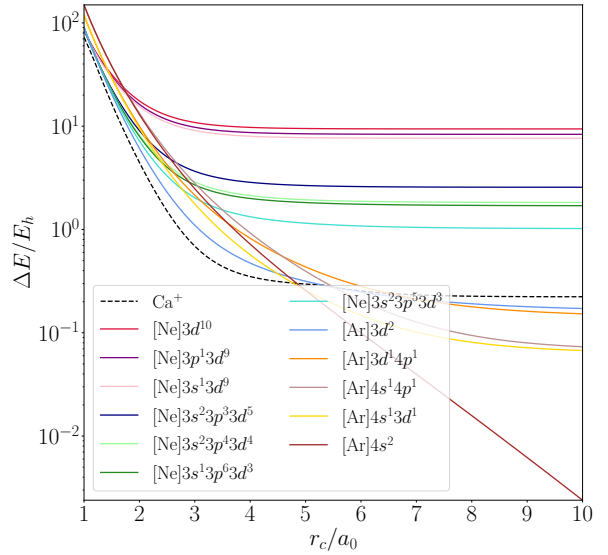


Figure 5: Energies of low lying configurations of hard-wall confined spin-polarized Ca computed with PBE shown as the energy difference from unconfined Ca as a function of the confinement radius. Note semilogarithmic scale.

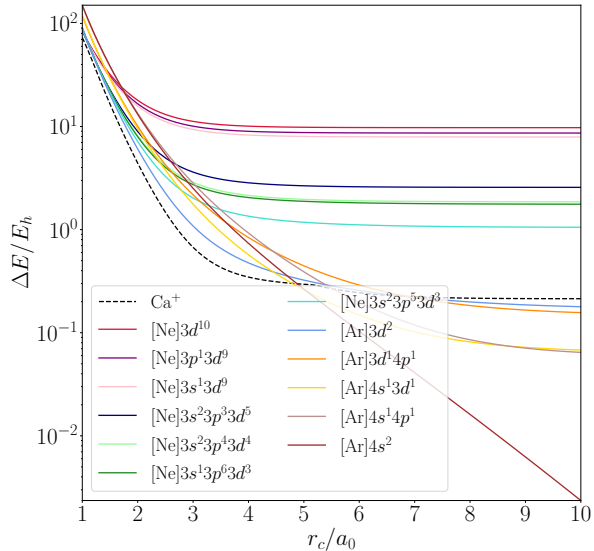


Figure 6: Energies of low lying configurations of hard-wall confined spin-polarized Ca computed with  $r^2$ SCAN shown as the energy difference from unconfined Ca as a function of the confinement radius. Note semilogarithmic scale.

the results of any of the other calculations for  $Z \geq 15$ . These surprisingly large differences are likely explained by the lack of electron correlation in Hartree–Fock theory, which is known to lead to overestimation of atoms’ size compared to high-level wave function calculations, with DFT yielding close agreement with accurate theoretical reference values.<sup>61</sup> The closeness of DFT densities with multideterminantal densities has also been noted on previously by [Ortiz-Henarejos and San-Fabián](#)<sup>62</sup>, for example.

Our calculations based on Janak’s theorem without the TSA systematically predict larger ionization radii than our  $\Delta$ SCF calculations, but they are still much smaller than the Hartree–Fock values of [Boeyens](#)<sup>5</sup>. Our  $\Delta$ SCF calculations are in excellent agreement with the limited data reported by [Sen et al.](#)<sup>15</sup> in the spin-restricted formalism, who also found good agreement between their TSA method and  $\Delta$ SCF calculations in their work. Interestingly, our spin-polarized data appears to be in better agreement with the calculations of [Sen et al.](#)<sup>15</sup> than our spin-restricted calculations, as the ad-

ditional comparisons included in the SI show, even though the calculations of [Sen et al.](#)<sup>15</sup> were spin-restricted. As was discussed in section 4.2.2, [Sen et al.](#)<sup>15</sup> did not include correlation in their calculations, which likely explains the differences between our data.

Our  $\Delta$ SCF calculations are also in good agreement for the 9 atoms studied by [Garza et al.](#)<sup>16</sup> with spin-polarized  $\Delta$ SCF calculations with the PW92 functional.

Since our  $\Delta$ SCF calculations were found to produce ionization potentials of unconfined atoms in good agreement with experimental values (section 4.1), and also yield ionization radii in good agreement between dissimilar density functional approximations as well as with previous literature, we are confident that our calculations offer thus a reliable basis for studies of confined atoms, and a reliable ground for further studies with elaborate wave function methods.

### 4.3 Estimates for atomic radii

Before proceeding to the in-depth analysis of the changes of atoms’ electronic structure in confinement, we return to the question of the atomic radii discussed above in section 2.4. Because the present study involves many configurations for each atom, many not being bound with respect to ionization in the unconfined atom, it is useful to be able to estimate the resulting atoms’ size. While the covalent size estimate of [Slater](#)<sup>45</sup> in eq. (9) is parameter-free, the two vdW radius estimates of eqs. (10) and (11) feature a threshold parameter.

[Bader et al.](#)<sup>46</sup> employed the threshold 0.002 electrons/bohr<sup>3</sup> in eq. (10), while [Boyd](#)<sup>63</sup> showed that the criterion 0.001 electrons/bohr<sup>3</sup> reproduces the same relative radii of atoms as those obtained with an even smaller value for the threshold. [Rahm et al.](#) also employed the threshold 0.001 electrons/bohr<sup>3</sup> in their study of atomic and ionic radii<sup>64,65</sup> and we chose to adopt this value of the threshold,  $\epsilon = 10^{-3}$  in eq. (10), as well. We note that [Smith et al.](#)<sup>66</sup> have also used eq. (10) recently to estimate vdW radii, opting to use a threshold of 0.0015 electrons/bohr<sup>3</sup>, instead.

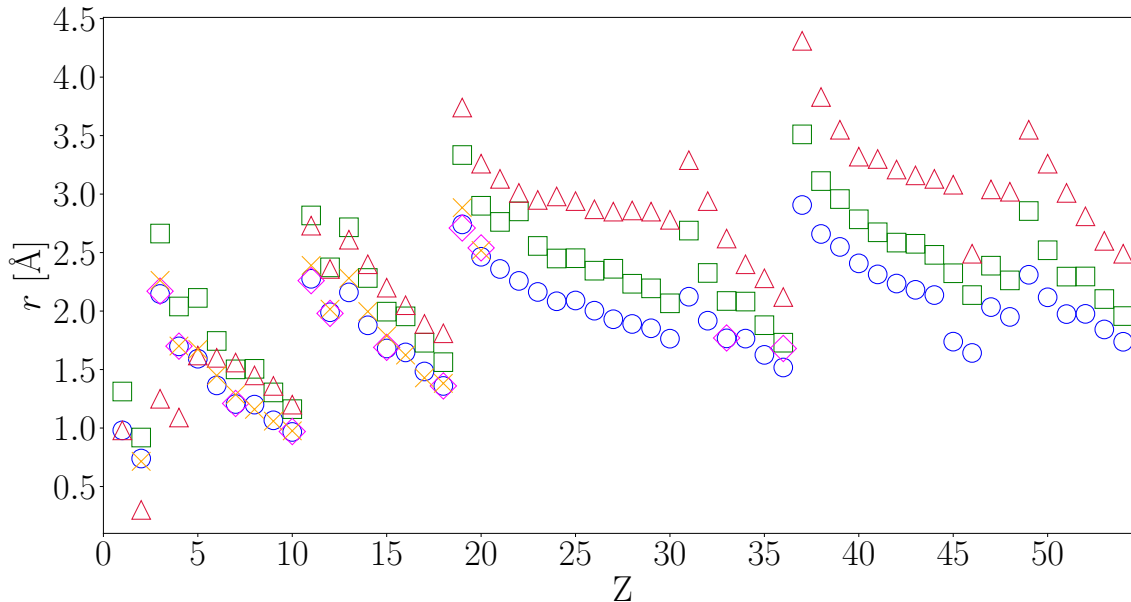


Figure 7: Comparison of ionization radii computed in this work with spin-polarized densities and the PBE density functional via  $\Delta$ SCF (blue circles) or Janak’s theorem (green squares) against the Hartree–Fock values of Boeyens<sup>5</sup> (red triangles) and DFT values of Sen et al.<sup>15</sup> (magenta diamonds) and Garza et al.<sup>16</sup> (orange crosses).

We discovered an issue in our analysis with the  $r_\rho$  estimate of eq. (10) for the vdW radius for the  $3d^1$  state of the H atom. As only  $s$ -type orbitals can have a finite value at the nucleus,<sup>48</sup> and as the  $3d$  orbital in question turns out to be extremely diffuse in character, the density criterion eq. (10) is not satisfied with any radius. As a result,  $r_\rho$  is not defined for the employed value of  $\epsilon$ .

In addition,  $r_\rho$  for the  $1s^1 3d^1$  configuration of He turns out to be smaller ( $r_\rho = 2.10a_0$  for spin-unrestricted PBE) than that for the  $1s^1 2p^1$  ( $r_\rho = 4.05a_0$ ) or  $1s^2$  ( $r_\rho = 2.68a_0$ ) configurations, even though basic physical insight would say that the  $1s^2$  ground state configuration has to be more compact than those where an electron is excited from the  $1s$  shell to the  $2p$  shell, not to mention to the  $3d$  shell.

We also find that the criterion of eq. (10) is overly sensitive to the numerical discretization: a finite element calculation for the exact ground state of the unconfined hydrogen atom reveals a significant sensitivity to numerical noise, as shown in fig. 8. We find it highly likely that similar issues are also present in the Gaussian-basis

calculations of refs. 64–66 that relied on the estimate of eq. (10): small changes to the Gaussian basis likely result in considerable changes in the estimated radius, since the calculations of fig. 8 which all reproduce the exact ground state energy  $-1/2E_h$  to sub- $\mu E_h$  accuracy exhibit considerable differences in the estimate of the vdW radius.

Note that the ANO-RCC basis set employed in refs. 64 and 65 produces an analogous Hartree–Fock energy of  $-0.49998374E_h$  (basis set obtained from the Basis Set Exchange<sup>67</sup> and calculation performed with ERKALE<sup>68</sup>), and thus exhibits a much larger truncation error of  $16.3\mu E_h$  for the unconfined hydrogen atom. Smith et al.<sup>66</sup> examined various Gaussian basis sets and variations in the order of  $0.01a_0$  can be observed in their data, as well.

To choose the criterion  $\epsilon$  in eq. (11), we match the two estimates of the vdW radius using the well-known analytical expression for the ground state of the hydrogen atom ( $R_{1s}(r) = 2e^{-r}$ ,  $f_{1s} = 1$ ). Performing the matching using 20-digit precision in Maple 2024, the electron density is found to be  $10^{-3}$  electrons/bohr<sup>3</sup> at

$r_\epsilon \approx 2.8815126965663684390a_0 \approx 1.524 \text{ \AA}$ , and evaluating eq. (11) yields the threshold  $\epsilon \approx 0.073416683704840394115$  electrons for use in determining the radius from eq. (11).

The data in fig. 8 show that the proposed  $r_\epsilon$  estimate of eq. (11) is numerically well-behaved, yielding excellent agreement with the radius determined from the analytical solution, thus successfully addressing the issues with undefined vdW radii and numerical stability in the  $r_\rho$  estimate of eq. (10). This criterion also easily resolves the issue with the configurations of He, agreeing with physical insight that the  $1s^2$  ground state ( $r_\epsilon = 2.26a_0$  for spin-unrestricted PBE) is more compact than the  $1s^2 2p^1$  ( $r_\epsilon = 8.07a_0$ ) or  $1s^1 3d^1$  ( $r_\epsilon = 15.48a_0$ ) excited states, the latter of which also show a significant difference in diffuse character.

The  $r_\epsilon$  estimates for the states of He are also in excellent qualitative agreement with the covalent radius estimates  $r_{\max}$  of eq. (9): both  $r_\epsilon$  and  $r_{\max}$  predict the size order  $1s^2 < 2p^2 < 1s^1 2p^1 < 1s^1 3d^1$ , while the  $r_\rho$  estimate of eq. (10) predicts a thoroughly dissimilar order  $1s^1 3d^1 < 1s^2 < 1s^1 2p^1 < 2p^2$ .

We note again here that the  $1s^1 3d^1$  excited state is so diffuse in the unconfined He atom that it is likely not converged to the complete basis set limit in our calculations, as we chose not to converge the value of the practical infinity  $r_\infty$  given that excited states of the unconfined atom are not the focus of this work.

## 4.4 Observed changes in electronic structure

In the following, we will discuss the key observations from the systematic analysis of all the atoms H–Xe. We focus the discussion in the main text on the PBE functional due to its insurmountable popularity in the literature, but note that the behaviors of various atoms are qualitatively independent of the functional, as was already demonstrated for the Ca atom in section 4.2. Thorough analyses for all functionals are available in the SI.

In addition to energies of the configurations as a function of confinement, we also report the estimated atomic radii for the configurations

of the unconfined atoms with the methodology discussed in sections 2.4 and 4.3 in the SI. We note again the limitations of the previously used  $r_\rho$  estimate of eq. (10) that was discussed above in section 4.3, in that the reported  $r_\rho$  values exhibit numerical noise. Furthermore, the excitation energies of each configuration relative to the ground state are also included in the SI for the case of the unconfined atom.

We note here that we were unable to converge the calculations of some configurations with the r<sup>2</sup>SCAN functional. We tentatively attribute this to the numerical ill-behavedness of the functional<sup>69</sup> and to the slow convergence of meta-GGA functionals in general with respect to the number of radial elements.<sup>33</sup> We have excluded all non-converged calculations from our analysis.

The in-depth analysis of the data included in the SI led us to the following observations on the behavior of the H–Xe atoms, which can be grouped into the following classification based on the atom’s position in the periodic table.

**H–He** Similarly to previous studies, we do not observe ground state crossings for the H or He atoms in the studied range of confinement radii. The  $1s$  orbital remains occupied over the whole domain of studied confinement radii. Interestingly, both atoms have configurations with an occupied  $3d$  orbital which are stable with respect to ionization in the unconfined atom (the configuration has a lower energy than that of the cation’s ground state), even though the  $3d$  orbital is extremely diffuse as  $r_\epsilon \approx 15a_0$  for the corresponding configuration.

**Li–O** The valence electrons of the Li–O atoms occupy the  $2s$  orbital in the unconfined atom. Contrary to the H and He atoms, we observe ground state crossings where the  $2s$  electrons hop to the  $2p$  orbital as the confinement radius is decreased; for the Li atom this happens already at  $r_c = 3a_0$ , but the location of the crossover point  $r_c$  decreases in increasing charge and occurs for the O atom at  $r_c = a_0$ .

The electron shift for Li was also predicted by Rahm et al.<sup>22</sup>, while the  $2s^2 \rightarrow 2p^2$  transition of the C atom was reported by Pařteka et al.<sup>19</sup>. As



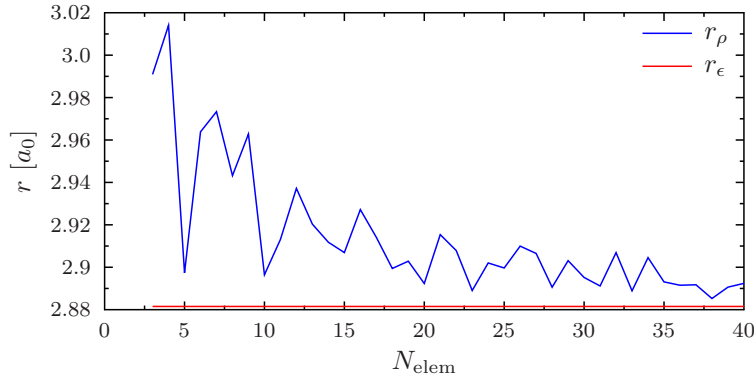


Figure 8: The dependence of the radial estimates  $r_{\rho}$  and  $r_{\epsilon}$  defined by eqs. (10) and (11), respectively, on the number of radial elements  $N_{\text{elem}}$  used in the discretization. The calculations are performed for the ground state of the hydrogen atom, using unrestricted Hartree–Fock theory, and the error in the total energy compared to the analytical value  $-0.5E_h$  is smaller than  $10^{-7}E_h$  in all calculations shown in the figure. The estimates from eq. (11) agree with the analytical value  $r_{\epsilon} \approx 2.8815126965663684390a_0$  to a precision better than one part per million.

far as we are aware, the analogous transitions for the Be, B, N, and O atoms have not been discussed in previous literature.

We further note that the Li and O atoms have configurations with an occupied  $3d$  orbital that are stable with respect to ionization in the unconfined atom, although the  $3d$  orbital is again extremely diffuse as  $r_{\epsilon} \approx 15a_0$ , as in the case of H and He.

**F** The valence electrons in the F atom occupy the  $2s$  and  $2p$  orbitals. One of the  $2s$  electrons hops to the  $2p$  orbital at  $r_c = a_0$ , which represents extreme confinement, thus fully filling the  $2p$  orbital. This electron transition does not appear to have been previously reported in the literature. Similarly to Li and O, F has a configuration with an occupied  $3d$  orbital already in the unconfined atom, but the orbital is equally diffuse.

**Ne** Confirming previous studies, the Ne atom does not exhibit ground state crossings in the studied range of confinement radii. We note that also Ne has a configuration with an occupied  $3d$  orbital which is stable with respect to ionization in the unconfined atom.

**Na–Mg** The valence electrons of Na and Mg occupy the  $3s$  orbital, which becomes un-

favourable in confinement, like the  $2s$  orbital in Li and Be. While in Li and Be the electrons hopped from  $2s$  to  $2p$ , the  $3s$  electrons of Na and Mg hop to the  $3d$  orbital around  $r_c \approx 2a_0$ , instead, even though the  $3d$  orbital has a larger extent than the  $3p$  orbital in the unconfined atom, and the  $3d$  orbital is not a valence orbital even in the Mg atom without confinement.<sup>70</sup> These electron transitions, which occur at relatively strong confinement, have not been previously reported in the literature to our knowledge.

We observe that the  $[\text{Ne}]4f$  configuration of the Na atom is stable with respect to ionization in the unconfined atom, and flips below the initial ground state in extreme confinement (close to  $r_c = a_0$ ). The  $4f$  orbital is highly diffuse in the unconfined atom ( $r_{\epsilon} \approx 24a_0$ ). Also the state  $[\text{Ne}]3d^14f^1$  of Mg flips below the initial ground state close to  $r_c = a_0$ .

**Al–Ar** The valence electrons of the unconfined Al–Ar atoms occupy the  $3s$  and  $3p$  orbitals. No electron shifts have been reported in previous studies for these atoms. However, we see that the  $3p$  orbital becomes unfavourable in confinement, gradually transferring all electrons to the  $3d$  orbital when the confinement radius is decreased, the transition occurring between  $r_c = 2a_0$  and  $r_c = 1.5a_0$  (strong confinement). As the confinement radius is further

decreased, both the  $3s$  electrons follow. The behavior is thus different from that observed above for Li–Ne, likely because the  $3d$  orbital is too high to be accessible in the lighter atoms.

**K–Ca** Confirming the results of previous studies,<sup>9,17,22</sup> analogously to Na and Mg, the  $4s$  valence electrons of the K and Ca atoms hop to the  $3d$  orbital around  $r_c \approx 4.5a_0$ . The  $3d$  orbital is thus already easily accessible, and its relevance in chemistry has been well established in the literature:<sup>70–76</sup> Ca is sometimes referred to in the literature as an “honorary transition metal”<sup>76</sup> due to its covalent binding like a transition metal,<sup>70,72,73,75</sup> following similar work performed earlier on the heavier analogues Cs and Ba which are not considered in this work.<sup>77</sup>

Further novel ground state crossings happen close to  $r_c = a_0$  (extreme confinement), where the [Ar] core configuration is opened up and all the  $3s$  and  $3p$  electrons also move to the  $3d$  orbital. We observe that both atoms have a configuration with an occupied  $3d$  orbital that is bound relative to ionization in the unconfined atom.

**Sc–Ni** The  $3d$  transition metals feature strong competition between the  $4s$  and  $3d$  orbitals, which can be observed from the small excitation energies in the unconfined atom. The states [Ar] $3d^n$ ,  $n \leq 10$  are stable with respect to ionization already in the unconfined atom, which explains why ground state crossings happen already in weak confinement.

Confirming previous findings,<sup>9,22</sup> the  $4s$  electrons shift to the  $3d$  orbital around  $r_c = 4a_0$  in the Sc–Ni atoms, similarly to the observations made above for K and Ca. However, here we observe that the Sc and Ti atoms exhibit additional ground state crossings in extreme confinement (between  $r_c = a_0$  and  $r_c = 2a_0$ ), where some  $3s$  and  $3p$  electrons also shift to the  $3d$  orbital.

**Cu–Zn** The unconfined Cu and Zn atoms already have a fully filled  $3d$  orbital in their ground states, thus the  $4s \rightarrow 3d$  shift observed earlier in the  $3d$  transition metal series can-

not happen for these atoms. The  $4s$  electrons hop to the  $4f$  orbital in extreme confinement (around  $r_c = 1.5a_0$ ), instead, which does not appear to have been previously reported in the literature.

**Ga–Kr** The ground state configurations of the unconfined Ga–Kr atoms have filled  $4s$  and  $3d$  orbitals and a variably filled  $4p$  orbital. The  $4s$  and  $4p$  electrons hop to the  $4f$  orbital as the confinement radius is decreased (between  $r_c = 1.5a_0$  and  $r_c = a_0$ ), leading to a [Ar] $3d^{10}4f^n$  ground state in extreme confinement. The favouring of the  $4f$  orbital over the  $4s$  and  $4p$  orbitals in the confined Kr atom has been previously reported by Garza et al.<sup>16</sup>.

**Rb–Sr** Like the alkali and earth alkali atoms in the previous period, the valence  $5s$  electrons of the Rb and Sr atoms hop to the  $4d$  orbital already around  $r_c = 5a_0$  confirming the previous observations of Guerra et al.<sup>17</sup> and Rahm et al.<sup>22</sup>. However, unlike the lighter analogues K and Ca, we also see a  $4d \rightarrow 4f$  shift when the confinement radius is further decreased to  $r_c \approx 1.2a_0$ , which represents extreme confinement. The  $4s$  and  $4p$  electrons also shift to the  $4f$  orbital below  $r_c = 1.2a_0$ , which, to the best of our knowledge, has not been reported in the literature so far.

**Y–Rh** The valence electrons of the unconfined Y–Rh atoms occupy the  $5s$  and  $4d$  orbitals in their ground states. The  $5s$  valence orbital becomes unfavourable in confinement, and the electrons hop to the  $4d$  orbital at confinement radii varying from  $r_c = 6.1a_0$  to  $r_c = 4.2a_0$ , that is, already in weak confinement, in agreement with previous literature.<sup>9,22</sup> Again, like for Cu–Sr, we observe further electron shifts to the  $4f$  orbital, and the  $4d$  orbital is partially depopulated after the  $5s$  orbital in confinement radii below  $r_c = 1.5a_0$ , which already represents extreme confinement. Y and Zr shift electrons from the  $4p$  core orbital to the  $4f$  orbital close to  $r_c = a_0$ . These additional electron shifts do not appear to have been reported in previous studies.

**Pd** It is well known that the unconfined Pd atom has a particularly stable ground state ( $[\text{Kr}]4d^{10}$ ).<sup>9,22</sup> We observe no ground state crossings for Pd in the studied range of confinement radii.

**Ag–Cd** Ag and Cd already have a filled  $4d$  orbital, while we observe previously unexplored electron shifts where  $5s$  electrons hop to the  $4f$  orbital around  $r_c = 2a_0$ .

**In–Xe** The In–Xe atoms have filled  $5s$  and  $4d$  orbitals and a  $5p$  orbital with variable filling in the unconfined atom. We observe that the  $5p$  electrons start to gradually shift to the  $4f$  orbital around  $r_c = 2a_0$ , after which both the  $5s$  electrons follow analogously to Ga–Kr, which does not appear to have been reported in the literature before now.

## 5 Summary and conclusion

To the best of our knowledge, a robust and systematic study of atoms in confinement has not been hitherto published in the literature. Such a study both needs to use a suitable numerical method and to consider the changing nature of the ground state as a function of the confinement. We did not find a single publication that satisfies both these criteria while also considering an appreciable portion of the periodic table instead of just some specific subrows or groups.

We therefore took a fully numerical approach based on the finite element method (FEM) to study atoms in hard-wall confinement. We chose to represent the atoms with spherically averaged, spin-restricted or spin-polarized densities, and carried out calculations at three levels of density functional approximations: the local density approximation employing the Perdew–Wang (PW92) correlation functional, the generalized-gradient approximation (GGA) employing the Perdew–Burke–Ernzerhof (PBE) exchange–correlation functional, and the meta-GGA approximation employing the  $r^2\text{SCAN}$  exchange–correlation functional. We compared the ionization energies of unconfined atoms predicted by spin-restricted or spin-polarized cal-

culations to experiment, and unsurprisingly observed the latter to be more accurate, while even the spin-restricted calculations succeed in predicting periodic trends.

We demonstrated the significance of considering confinement induced changes in the electronic structure by comparing ionization radii computed for fixed electron configurations to those obtained in calculations in which the electron configuration can relax as a function of the confinement radius. Depending on the atom, this relaxation can result in either an increase or a decrease of the ionization radius due to competing effects in the neutral atom and its cation, and the largest differences are seen for the pre- $d$  and early  $d$  elements.

As a side result of our study, we also examined various atomic size estimates. We found severe issues in the van der Waals (vdW) radius estimate proposed by Bader et al.<sup>46</sup>: it is not always defined, it has severe issues with numerical stability even with huge numerical basis sets, and its predictions do not agree with basic physical insights for the  $1s^2$  ground and  $1s^12p^1$  and  $1s^13d^1$  excited configurations of the He atom. We proposed a related estimate which is always defined, does not suffer from severe numerical problems like the aforementioned estimate, and also predicts the aforementioned states of the He atom to be increasingly diffuse in character, in agreement with the covalent radius estimate of Slater<sup>45</sup>. We expect our proposed vdW radius estimate to be useful in future work.

We then carried out a systematic study of the total energies of the ground and low lying excited states of the H–Xe atoms as well as their monocations as a function of the confinement radius  $r_c$ , paying special focus on how the ground state evolves as a function of confinement. We have confirmed electron shifts made in previous studies on confined atoms, but also made novel observations. We summarize our analysis of the calculations as follows.

- Ground state crossings occur for the majority of the elements.
- Valence  $s$  electrons are highly unfavoured under strong confinement: already the Li

and Be atoms show a  $2s \rightarrow 2p$  electron shift.

- Shifts from the  $ns$  and  $np$  to the  $3d$  orbital are observed for the elements of the second and third periods.
- Shifts to the  $4f$  orbital can be observed for Cu onwards in strong confinement.

Importantly, we saw that the dissimilar density functional approximations were in excellent agreement in calculations of ionization radii, and that the qualitative behavior of the confined atoms is similar for dissimilar density functionals. We are therefore confident that our results are not artefacts of the employed level of theory, and that similar results would be obtained even with high-level *ab initio* calculations.

Like most studies on confined atoms, the present study was limited to the use of integer occupation numbers for the  $s$ ,  $p$ ,  $d$ , and  $f$  shells to maximize physical interpretability. However, as we discussed in section 4.2.2, the use of non-integral occupation numbers could be useful for transition metals, for instance,<sup>32,42,43</sup> and we hope to revisit such calculations with state-of-the-art optimization algorithms such as optimal damping<sup>78</sup> in future work.

Our study was limited to the H–Xe atoms, because relativistic effects are well known to be essential for heavy elements.<sup>79,80</sup> Relativistic calculations of atoms in confinement should be feasible using the same approach, and such calculations might be carried out with the recent implementation of Čertík et al.<sup>81</sup>, for example.

## 5.1 Connections to basis set design

It is interesting to draw a parallel here to basis set design, since the application of confinement potentials in the construction of numerical atomic orbital (NAO) basis sets as originally proposed by by Averill and Ellis<sup>82</sup> was the original motivation of our work. While Averill and Ellis<sup>82</sup> employed a finite potential barrier, Sankey and Niklewski<sup>83</sup> proposed building NAO basis sets using a hard-wall poten-

tial to enforce the locality of the resulting basis set. In later works, Sankey and coworkers refer to the arising orbitals as “fireballs” due to their excited nature relative to the unconfined atom.<sup>84,85</sup> The technique of Sankey and Niklewski<sup>83</sup> has been later used by many other authors as well, such as Sánchez-Portal et al.<sup>86</sup>, Basanta et al.<sup>87</sup>, Kenny and Horsfield<sup>88</sup>, and Nakata et al.<sup>89</sup>.

The demands for various chemical elements’ atomic orbital basis sets for electronic structure calculations<sup>90–92</sup> are inherently tied to the elements’ chemistry. Importantly, the relevance of distinct angular momentum  $l$  orbitals for atoms is expected to be a continuous function: as we move to heavier elements, we first see an increasing importance of  $p$  functions, followed by increasing importance of  $d$  functions,  $f$  functions and so on. Unlike the occupied orbitals in an SCF calculation on an atom, the importance of polarization functions in a basis set is not a step function for which we can certainly say whether a specific element requires  $s$ ,  $p$ ,  $d$ ,  $f$ , etc. functions, or not.

This continuity is a challenge when predicting the relevance of distinct orbitals to chemical bonding. The advantage of our arguably simple model is that we are able to highlight these chemical characteristics of the studied atoms, that is, the *relative* importance of the electron configurations as a function of confinement. The physicality of the model is therefore obvious. For example, we saw in this work that the simple hard-wall confinement model predicts the importance of the  $3d$  orbital in K and Ca, which is obvious from the large transition radius  $r_c \approx 4.5a_0$ .

In contrast, the  $3d$  orbital is so high in the second-row  $3p$  block that electron shifts to it only occur in strong confinement. Yet, it is by now well known<sup>93–98</sup> that tight  $d$  functions need to be included in the basis set for the second-row  $p$  block elements in polyatomic electronic structure calculations, as this inclusion typically results in significant increases of atomization energies: for example, the atomization energies of sulfur containing molecules such as  $\text{SO}_2$  and  $\text{SO}_3$  typically increase by tens of kcal/mol upon the addition of  $3d$  functions.

Perchloric acid ( $\text{HClO}_4$ ) and dichlorine heptoxide ( $\text{Cl}_2\text{O}_7$ ) represent even more extreme cases, with documented increases of the atomization energy by 50 and 100 kcal/mol, respectively.<sup>99</sup>

Martin<sup>99</sup> found a physical interpretation for this effect: the  $3d$  Rydberg orbital on the chlorine atom(s) can accept back-bonding contributions from the oxygen atoms. Mehta and Martin<sup>100</sup> also point out that the  $3d$  orbital comes down in energy when the atom becomes more positively charged. Indeed, atomic orbitals determined for cations are commonly used to introduce additional flexibility in NAO basis sets.<sup>101</sup> Mehta and Martin<sup>100</sup> also made the discovery that the fourth-row  $5p$  block analogously exhibits a heightened importance of  $4f$  Rydberg orbitals.

Based on the above findings, we expect that heavier elements will exhibit electron shifts to the  $4f$  orbital in weaker and weaker confinement, since the  $4f$  orbital will come down in energy as the nuclear charge is increased.

**Acknowledgement** We thank professor Pekka Pyykkö for comments on the manuscript, and Monica Lindholm for designing the cover graphics for the manuscript. H.Å. thanks the Finnish Society for Sciences and Letters for funding. S.L. thanks the Academy of Finland for financial support under project numbers 350282 and 353749.

## Supporting Information Available

The SI PDF file contains the following data. Comparison of the ionization energies with the PW92 and  $r^2\text{SCAN}$  functional. Values of the ionization radii via Janak's theorem for both the fixed and relaxed configuration approaches. Detailed analysis of the evolution of the ground state of the H–Xe atoms, and state crossings with the ground state configuration of the unconfined atom. Estimated atomic sizes and excitation energies relative to the ground state for the studied configurations in the unconfined atom. Plots of the total energy of the low lying states of the H–Xe atoms and their monoca-

tions as a function of the confinement radius. All of the above sets of results are given both for the spin-restricted and spin-polarized formalisms for all the functionals considered in this work: PW92, PBE, and  $r^2\text{SCAN}$ . The raw energies for all calculations are included in comma separated values (CSV) format in a compressed archive.

## References

- (1) Michels, A.; De Boer, J.; Bijl, A. Remarks concerning molecular interaction and their influence on the polarisability. *Physica* **1937**, *4*, 981–994.
- (2) Aquino, N. The Hydrogen and Helium Atoms Confined in Spherical Boxes. *Adv. Quantum Chem.* **2009**, *57*, 123–171.
- (3) Lehtola, S.; Dimitrova, M.; Sundholm, D. Fully numerical electronic structure calculations on diatomic molecules in weak to strong magnetic fields. *Mol. Phys.* **2020**, *118*, e1597989.
- (4) Åström, H.; Lehtola, S. Insight on Gaussian Basis Set Truncation Errors in Weak to Intermediate Magnetic Fields with an Approximate Hamiltonian. *J. Phys. Chem. A* **2023**, *127*, 10872–10888.
- (5) Boeyens, J. C. A. Ionization radii of compressed atoms. *J. Chem. Soc., Faraday Trans.* **1994**, *90*, 3377.
- (6) Chattaraj, P. K.; Sarkar, U. Chemical reactivity of the spherically confined atoms. *Chem. Phys. Lett.* **2003**, *372*, 805–809.
- (7) Chattaraj, P. K.; Sarkar, U. Effect of Spherical Confinement on Chemical Reactivity. *J. Phys. Chem. A* **2003**, *107*, 4877–4882.
- (8) Sarkar, U.; Giri, S.; Chattaraj, P. K. Dirichlet Boundary Conditions and Effect of Confinement on Chemical Reactivity. *J. Phys. Chem. A* **2009**, *113*, 10759–10766.

- (9) Connerade, J. P.; Dolmatov, V. K.; Lakshmi, P. A. The filling of shells in compressed atoms. *J. Phys. B: At., Mol. Opt. Phys.* **2000**, *33*, 251–264.
- (10) Connerade, J. P.; Dolmatov, V. K. Controlling orbital collapse from inside and outside a transition element. *J. Phys. B: At., Mol. Opt. Phys.* **1998**, *31*, 3557–3564.
- (11) Connerade, J.-P.; Semaoune, R. Relativistic study of the electronic structure and  $5d$  orbital of La confined inside a  $C_{60}$  fullerene cage. *J. Phys. B: At. Mol. Opt. Phys.* **2000**, *33*, 869–880.
- (12) Connerade, J. P.; Semaoune, R. Atomic compressibility and reversible insertion of atoms into solids. *J. Phys. B: At., Mol. Opt. Phys.* **2000**, *33*, 3467–3484.
- (13) Garza, J.; Vargas, R.; Vela, A. Numerical self-consistent-field method to solve the Kohn–Sham equations in confined many-electron atoms. *Phys. Rev. E* **1998**, *58*, 3949–3954.
- (14) Garza, J.; Vargas, R.; Vela, A.; Sen, K. D. Shell structure in free and confined atoms using the density functional theory. *J. Mol. Struct.: THEOCHEM* **2000**, *501-502*, 183–188.
- (15) Sen, K. D.; Garza, J.; Vargas, R.; Vela, A. Atomic ionization radii using Janak’s theorem. *Chem. Phys. Lett.* **2000**, *325*, 29–32.
- (16) Garza, J.; Vargas, R.; Aquino, N.; Sen, K. D. DFT reactivity indices in confined many-electron atoms. *J. Chem. Sci.* **2005**, *117*, 379–386.
- (17) Guerra, D.; Vargas, R.; Fuentealba, P.; Garza, J. Modeling Pressure Effects on the Electronic Properties of Ca, Sr, and Ba by the Confined Atoms Model. *Adv. Quantum Chem.* **2009**, *58*, 1–12.
- (18) Lozano-Espinosa, M.; Garza, J.; Galván, M. Confinement effects on the spin potential of first row transition metal cations. *Philos. Mag.* **2017**, *97*, 284–297.
- (19) Pašteka, L. F.; Helgaker, T.; Saue, T.; Sundholm, D.; Werner, H.-J.; Hasanbulli, M.; Major, J.; Schwerdtfeger, P. Atoms and molecules in soft confinement potentials. *Mol. Phys.* **2020**, *118*, e1730989.
- (20) Roos, B. O. The complete active space SCF method in a Fock-matrix-based super-CI formulation. *Int. J. Quantum Chem.* **1980**, *18*, 175–189.
- (21) Roos, B. O.; Taylor, P. R.; Siegbahn, P. E. M. A complete active space SCF method (CASSCF) using a density matrix formulated super-CI approach. *Chem. Phys.* **1980**, *48*, 157–173.
- (22) Rahm, M.; Cammi, R.; Ashcroft, N. W.; Hoffmann, R. Squeezing All Elements in the Periodic Table: Electron Configuration and Electronegativity of the Atoms under Compression. *J. Am. Chem. Soc.* **2019**, *141*, 10253–10271.
- (23) Cammi, R. A new extension of the polarizable continuum model: Toward a quantum chemical description of chemical reactions at extreme high pressure. *J. Comput. Chem.* **2015**, *36*, 2246–2259.
- (24) (a) Widmark, P.-O.; Malmqvist, P.-Å.; Roos, B. O. Density matrix averaged atomic natural orbital (ANO) basis sets for correlated molecular wave functions. I. First row atoms. *Theor. Chim. Acta* **1990**, *77*, 291–306; (b) Roos, B. O.; Veryazov, V.; Widmark, P.-O. Relativistic atomic natural orbital type basis sets for the alkaline and alkaline-earth atoms applied to the ground-state potentials for the corresponding dimers. *Theor. Chem. Acc.* **2004**, *111*, 345–351; (c) Roos, B. O.; Lindh, R.; Malmqvist, P.-Å.; Veryazov, V.; Widmark, P.-O. Main Group Atoms and Dimers Studied with a New Relativistic ANO Basis Set.

- J. Phys. Chem. A* **2004**, *108*, 2851–2858; (d) Roos, B. O.; Lindh, R.; Malmqvist, P.-Å.; Veryazov, V.; Widmark, P.-O. New relativistic ANO basis sets for transition metal atoms. *J. Phys. Chem. A* **2005**, *109*, 6575–9; (e) Roos, B. O.; Lindh, R.; Malmqvist, P.-Å.; Veryazov, V.; Widmark, P.-O. New relativistic ANO basis sets for actinide atoms. *Chem. Phys. Lett.* **2005**, *409*, 295–299; (f) Roos, B. O.; Lindh, R.; Malmqvist, P.-Å.; Veryazov, V.; Widmark, P.-O.; Borin, A. C. New relativistic atomic natural orbital basis sets for lanthanide atoms with applications to the Ce diatom and LuF<sub>3</sub>. *J. Phys. Chem. A* **2008**, *112*, 11431–11435.
- (25) Ernzerhof, M.; Scuseria, G. E. Assessment of the Perdew–Burke–Ernzerhof exchange–correlation functional. *J. Chem. Phys.* **1999**, *110*, 5029–5036.
- (26) Adamo, C.; Barone, V. Toward reliable density functional methods without adjustable parameters: The PBE0 model. *J. Chem. Phys.* **1999**, *110*, 6158–6170.
- (27) Perdew, J. P.; Burke, K.; Ernzerhof, M. Generalized Gradient Approximation Made Simple. *Phys. Rev. Lett.* **1996**, *77*, 3865–3868.
- (28) Perdew, J. P.; Burke, K.; Ernzerhof, M. Generalized Gradient Approximation Made Simple [Phys. Rev. Lett. *77*, 3865 (1996)]. *Phys. Rev. Lett.* **1997**, *78*, 1396–1396.
- (29) Rahm, M.; Ångqvist, M.; Rahm, J. M.; Erhart, P.; Cammi, R. Non-Bonded Radii of the Atoms Under Compression. *ChemPhysChem* **2020**, *21*, 2441–2453.
- (30) Hohenberg, P.; Kohn, W. Inhomogeneous Electron Gas. *Phys. Rev.* **1964**, *136*, B864–B871.
- (31) Kohn, W.; Sham, L. J. Self-Consistent Equations Including Exchange and Correlation Effects. *Phys. Rev.* **1965**, *140*, A1133–A1138.
- (32) Lehtola, S. Fully numerical calculations on atoms with fractional occupations and range-separated exchange functionals. *Phys. Rev. A* **2020**, *101*, 012516.
- (33) Lehtola, S. Meta-GGA Density Functional Calculations on Atoms with Spherically Symmetric Densities in the Finite Element Formalism. *J. Chem. Theory Comput.* **2023**, *19*, 2502–2517.
- (34) Bagus, P. S.; Bennett, B. I. Singlet–triplet splittings as obtained from the  $X\alpha$ -scattered wave method: A theoretical analysis. *Int. J. Quantum Chem.* **1975**, *9*, 143–148.
- (35) Ziegler, T.; Rauk, A.; Baerends, E. J. On the calculation of multiplet energies by the Hartree–Fock–Slater method. *Theor. Chim. Acta* **1977**, *43*, 261–271.
- (36) von Barth, U. Local-density theory of multiplet structure. *Phys. Rev. A* **1979**, *20*, 1693–1703.
- (37) Wood, J. H. Atomic multiplet structures obtained from Hartree–Fock, statistical exchange and local spin density approximations. *J. Phys. B At. Mol. Phys.* **1980**, *13*, 1–14.
- (38) Nagy, Á. Kohn–Sham equations for multiplets. *Phys. Rev. A* **1998**, *57*, 1672–1677.
- (39) Baerends, E. J.; Branchadell, V.; Sodupe, M. Atomic reference energies for density functional calculations. *Chem. Phys. Lett.* **1997**, *265*, 481–489.
- (40) Koopmans, T. Über die Zuordnung von Wellenfunktionen und Eigenwerten zu den einzelnen Elektronen eines Atoms. *Physica* **1934**, *1*, 104–113.
- (41) Janak, J. Proof that  $\partial E/\partial n_i = \epsilon_i$  in density-functional theory. *Phys. Rev. B* **1978**, *18*, 7165–7168.
- (42) Slater, J. C.; Mann, J. B.; Wilson, T. M.; Wood, J. H. Nonintegral Occupation

- Numbers in Transition Atoms in Crystals. *Phys. Rev.* **1969**, *184*, 672–694.
- (43) Kraisler, E.; Makov, G.; Kelson, I. Ensemble  $\nu$ -representable ab initio density-functional calculation of energy and spin in atoms: A test of exchange-correlation approximations. *Phys. Rev. A* **2010**, *82*, 042516.
- (44) Cancès, E.; Mourad, N. A numerical study of the extended Kohn–Sham ground states of atoms. *Comm. App. Math. Com. Sc.* **2018**, *13*, 139–188.
- (45) Slater, J. C. Atomic Shielding Constants. *Phys. Rev.* **1930**, *36*, 57–64.
- (46) Bader, R. F. W.; Henneker, W. H.; Cade, P. E. Molecular Charge Distributions and Chemical Binding. *J. Chem. Phys.* **1967**, *46*, 3341–3363.
- (47) Lehtola, S. A review on non-relativistic, fully numerical electronic structure calculations on atoms and diatomic molecules. *Int. J. Quantum Chem.* **2019**, *119*, e25968.
- (48) Lehtola, S. Fully numerical Hartree–Fock and density functional calculations. I. Atoms. *Int. J. Quantum Chem.* **2019**, *119*, e25945.
- (49) Lehtola, S. Atomic Electronic Structure Calculations with Hermite Interpolating Polynomials. *J. Phys. Chem. A* **2023**, *127*, 4180–4193.
- (50) Lehtola, S.; Karttunen, A. J. Free and open source software for computational chemistry education. *Wiley Interdiscip. Rev. Comput. Mol. Sci.* **2022**, *12*, e1610.
- (51) Lehtola, S. HelFEM—Finite element methods for electronic structure calculations on small systems. 2024; <http://github.com/susilehtola/HelFEM>, Accessed 10 June 2024.
- (52) Bloch, F. Bemerkung zur Elektronentheorie des Ferromagnetismus und der elektrischen Leitfähigkeit. *Z. Phys.* **1929**, *57*, 545–555.
- (53) Dirac, P. A. M. Note on Exchange Phenomena in the Thomas Atom. *Math. Proc. Cambridge Philos. Soc.* **1930**, *26*, 376–385.
- (54) Perdew, J. P.; Wang, Y. Accurate and simple analytic representation of the electron-gas correlation energy. *Phys. Rev. B* **1992**, *45*, 13244–13249.
- (55) Furness, J. W.; Kaplan, A. D.; Ning, J.; Perdew, J. P.; Sun, J. Accurate and Numerically Efficient r<sup>2</sup>SCAN Meta-Generalized Gradient Approximation. *J. Phys. Chem. Lett.* **2020**, *11*, 8208–8215.
- (56) Furness, J. W.; Kaplan, A. D.; Ning, J.; Perdew, J. P.; Sun, J. Correction to "Accurate and Numerically Efficient r<sup>2</sup>SCAN Meta-Generalized Gradient Approximation". *J. Phys. Chem. Lett.* **2020**, *11*, 9248–9248.
- (57) Lehtola, S.; Steigemann, C.; Oliveira, M. J. T.; Marques, M. A. L. Recent developments in LIBXC—a comprehensive library of functionals for density functional theory. *SoftwareX* **2018**, *7*, 1–5.
- (58) Kramida, A.; Yu. Ralchenko; Reader, J.; NIST ASD Team NIST Atomic Spectra Database (version 5.11). NIST Atomic Spectra Database (ver. 5.11), [Online]. Available: <https://physics.nist.gov/asd> [2024, July 4]. National Institute of Standards and Technology, Gaithersburg, MD., 2023.
- (59) Sommerfeld, A.; Welker, H. Künstliche Grenzbedingungen beim Keplerproblem. *Ann. Phys. (Berl.)* **1938**, *424*, 56–65.
- (60) Becke, A. D. Density-functional exchange-energy approximation with correct asymptotic behavior. *Phys. Rev. A* **1988**, *38*, 3098–3100.



- (61) Cohen, A. J.; Handy, N. C.; Roos, B. O. Are Hartree–Fock atoms too small or too large? *Phys. Chem. Chem. Phys.* **2004**, *6*, 2928–2931.
- (62) Ortiz-Henarejos, E.; San-Fabián, E. Differences between ab initio and density functional electron densities. *Int. J. Quantum Chem.* **1997**, *61*, 245–252.
- (63) Boyd, R. J. The relative sizes of atoms. *J. Phys. B: At. Mol. Phys.* **1977**, *10*, 2283–2291.
- (64) Rahm, M.; Hoffmann, R.; Ashcroft, N. W. Atomic and Ionic Radii of Elements 1–96. *Chem. Eur. J.* **2016**, *22*, 14625–14632.
- (65) Rahm, M.; Hoffmann, R.; Ashcroft, N. W. Corrigendum: Atomic and Ionic Radii of Elements 1–96. *Chem. Eur. J.* **2017**, *23*, 4017–4017.
- (66) Smith, M.; Li, Z.; Landry, L.; Merz, K. M.; Li, P. Consequences of Overfitting the van der Waals Radii of Ions. *J. Chem. Theory Comput.* **2023**, *19*, 2064–2074.
- (67) Pritchard, B. P.; Altarawy, D.; Didier, B.; Gibson, T. D.; Windus, T. L. New Basis Set Exchange: An Open, Up-to-Date Resource for the Molecular Sciences Community. *J. Chem. Inf. Model.* **2019**, *59*, 4814–4820.
- (68) Lehtola, J.; Hakala, M.; Sakko, A.; Hämmäläinen, K. ERKALE – A flexible program package for X-ray properties of atoms and molecules. *J. Comput. Chem.* **2012**, *33*, 1572–1585.
- (69) Lehtola, S.; Marques, M. A. L. Many recent density functionals are numerically ill-behaved. *J. Chem. Phys.* **2022**, *157*, 174114.
- (70) Fernández, I.; Holzmann, N.; Frenking, G. The Valence Orbitals of the Alkaline-Earth Atoms. *Chem. Eur. J.* **2020**, *26*, 14194–14210.
- (71) Pyykkö, P. Dirac–Fock one-centre calculations. Part 7. – Divalent systems  $MH^+$  and  $MH_2$  ( $M = Be, Mg, Ca, Sr, Ba, Ra, Zn, Cd, Hg, Yb$  and  $No$ ). *J. Chem. Soc., Faraday Trans. 2* **1979**, *75*, 1256–1276.
- (72) Wu, X.; Zhao, L.; Jin, J.; Pan, S.; Li, W.; Jin, X.; Wang, G.; Zhou, M.; Frenking, G. Observation of alkaline earth complexes  $M(CO)_8$  ( $M = Ca, Sr, \text{ or } Ba$ ) that mimic transition metals. *Science* **2018**, *361*, 912–916.
- (73) Zhou, M.; Frenking, G. Transition-Metal Chemistry of the Heavier Alkaline Earth Atoms Ca, Sr, and Ba. *Acc. Chem. Res.* **2021**, *54*, 3071–3082.
- (74) Liu, R.; Qin, L.; Zhang, Z.; Zhao, L.; Sagan, F.; Mitoraj, M.; Frenking, G. Genuine quadruple bonds between two main-group atoms. Chemical bonding in  $AeF^-$  ( $Ae = Be\text{--}Ba$ ) and isoelectronic  $EF$  ( $E = B\text{--}Tl$ ) and the particular role of d orbitals in covalent interactions of heavier alkaline-earth atoms. *Chem. Sci.* **2023**, *14*, 4872–4887.
- (75) Cui, L.; Liu, Y.; Wang, M.; Yan, B.; Pan, S.; Cui, Z.; Frenking, G. Multiple Bonding in  $AeN^-$  ( $Ae = Ca, Sr, Ba$ ). *Chem. Eur. J.* **2024**, *30*, e202400714.
- (76) Liu, X.-b.; Tiznado, W.; Cui, L.-J.; Barroso, J.; Leyva-Parra, L.; Miao, L.-h.; Zhang, H.-y.; Pan, S.; Merino, G.; Cui, Z.-h. Exploring the Use of “Honorary Transition Metals” To Push the Boundaries of Planar Hypercoordinate Alkaline-Earth Metals. *J. Am. Chem. Soc.* **2024**, *146*, 16689–16697.
- (77) Gagliardi, L.; Pyykkö, P. Cesium and barium as honorary d elements:  $CsN_7Ba$  as an example. *Theor. Chem. Acc.* **2003**, *110*, 205–210.
- (78) Cancès, E. Self-consistent field algorithms for Kohn–Sham models with fractional occupation numbers. *J. Chem. Phys.* **2001**, *114*, 10616–10622.

- (79) Pyykkö, P. Relativistic effects in chemistry: more common than you thought. *Annu. Rev. Phys. Chem.* **2012**, *63*, 45–64.
- (80) Pyykkö, P. The physics behind chemistry and the periodic table. *Chem. Rev.* **2012**, *112*, 371–84.
- (81) Čertík, O.; Pask, J. E.; Fernando, I.; Goswami, R.; Sukumar, N.; Collins, L. A.; Manzini, G.; Vackář, J. High-order finite element method for atomic structure calculations. *Comput. Phys. Commun.* **2024**, *297*, 109051.
- (82) Averill, F. W.; Ellis, D. E. An efficient numerical multicenter basis set for molecular orbital calculations: Application to FeCl<sub>4</sub>. *J. Chem. Phys.* **1973**, *59*, 6412–6418.
- (83) Sankey, O.; Niklewski, D. Ab initio multicenter tight-binding model for molecular-dynamics simulations and other applications in covalent systems. *Phys. Rev. B* **1989**, *40*, 3979–3995.
- (84) Lewis, J.; Glaesemann, K.; Voth, G.; Fritsch, J.; Demkov, A.; Ortega, J.; Sankey, O. Further developments in the local-orbital density-functional-theory tight-binding method. *Phys. Rev. B* **2001**, *64*, 195103.
- (85) Lewis, J. P.; Jelínek, P.; Ortega, J.; Demkov, A. A.; Trabada, D. G.; Haycock, B.; Wang, H.; Adams, G.; Tomfohr, J. K.; Abad, E. et al. Advances and applications in the FIREBALL ab initio tight-binding molecular-dynamics formalism. *Phys. Status Solidi B* **2011**, *248*, 1989–2007.
- (86) Sánchez-Portal, D.; Ordejón, P.; Artacho, E.; Soler, J. M. Density-functional method for very large systems with LCAO basis sets. *Int. J. Quantum Chem.* **1997**, *65*, 453–461.
- (87) Basanta, M. A.; Dappe, Y. J.; Jelínek, P.; Ortega, J. Optimized atomic-like orbitals for first-principles tight-binding molecular dynamics. *Comput. Mater. Sci.* **2007**, *39*, 759–766.
- (88) Kenny, S. D.; Horsfield, A. P. Plato: A localised orbital based density functional theory code. *Comput. Phys. Commun.* **2009**, *180*, 2616–2621.
- (89) Nakata, A.; Baker, J. S.; Mujahed, S. Y.; Poulton, J. T. L.; Arapan, S.; Lin, J.; Raza, Z.; Yadav, S.; Truflandier, L.; Miyazaki, T. et al. Large scale and linear scaling DFT with the CONQUEST code. *J. Chem. Phys.* **2020**, *152*, 164112.
- (90) Davidson, E. R.; Feller, D. Basis set selection for molecular calculations. *Chem. Rev.* **1986**, *86*, 681–696.
- (91) Jensen, F. Atomic orbital basis sets. *Wiley Interdiscip. Rev. Comput. Mol. Sci.* **2013**, *3*, 273–295.
- (92) Hill, J. G. Gaussian basis sets for molecular applications. *Int. J. Quantum Chem.* **2013**, *113*, 21–34.
- (93) Curtiss, L. A.; Jones, C.; Trucks, G. W.; Raghavachari, K.; Pople, J. A. Gaussian-1 theory of molecular energies for second-row compounds. *J. Chem. Phys.* **1990**, *93*, 2537.
- (94) Curtiss, L. A.; Raghavachari, K.; Trucks, G. W.; Pople, J. A. Gaussian-2 theory for molecular energies of first- and second-row compounds. *J. Chem. Phys.* **1991**, *94*, 7221–7230.
- (95) Bauschlicher, C. W.; Partridge, H. The sensitivity of B3LYP atomization energies to the basis set and a comparison of basis set requirements for CCSD(T) and B3LYP. *Chem. Phys. Lett.* **1995**, *240*, 533–540.
- (96) Martin, J. M. L. Basis set convergence study of the atomization energy, geometry, and anharmonic force field of SO<sub>2</sub>: The importance of inner polarization functions. *J. Chem. Phys.* **1998**, *108*, 2791–2800.

- (97) Martin, J. M. L. Heat of atomization of sulfur trioxide,  $\text{SO}_3$ : a benchmark for computational thermochemistry. *Chem. Phys. Lett.* **1999**, *310*, 271–276.
- (98) Dunning, T. H.; Peterson, K. A.; Wilson, A. K. Gaussian basis sets for use in correlated molecular calculations. X. The atoms aluminum through argon revisited. *J. Chem. Phys.* **2001**, *114*, 9244.
- (99) Martin, J. M. L. Heats of formation of perchloric acid,  $\text{HClO}_4$ , and perchloric anhydride,  $\text{Cl}_2\text{O}_7$ . Probing the limits of W1 and W2 theory. *J. Mol. Struct.: THEOCHEM* **2006**, *771*, 19–26.
- (100) Mehta, N.; Martin, J. M. L. The Importance of Tight f Basis Functions for Heavy p-Block Oxides and Halides: A Parallel With Tight d functions in the Second Row. *J. Phys. Chem. A* **2023**, *127*, 2104–2112.
- (101) Delley, B. An all-electron numerical method for solving the local density functional for polyatomic molecules. *J. Chem. Phys.* **1990**, *92*, 508.

# TOC Graphic

